

Anonymous Referee #1

Received and published: 26 November 2020

This manuscript provides a description of an inverse method based on the NH₃ lifetime to estimate NH₃ global emissions from the satellite IASI observations over the 10 yr-period 2008-2017. As NH₃ is a key species for understanding the PM levels, the quantification of its global emissions is important and would be useful to a wide community. The authors cover an important topic, appropriate for ACP. Nevertheless, I have some major comments listed below that should be considered by the authors before publication.

Response: We acknowledge reviewer's effort to improve our manuscript.

Major comments:

1/ The fact that NH₃ columns in the atmosphere depend not only on NH₃ emissions, but is also linked to the abundance of nitric and sulfuric acids (and consequently to NO_x and SO₂ emissions) is not fully described. To tackle the large variability of the ammonia lifetime, the authors calculated the NH₃ lifetime with a CTM and the spatial variability of ammonia is taken into account. I have more doubt about the temporal variability of ammonia and its main drivers in the atmosphere. If I well understand, the variable lifetime chosen for this study is a gridded average over the 10-yr period. If it is correct, the temporal trend in nitric and sulfuric acids is not fully taken into account, while it could have an importance for the deduced NH₃ emissions over a 10-yr period. This choice should be explained in the text. Would it possible to calculate yearly lifetimes as a sensitivity test to assess the robustness of your study?

Response: We appreciate reviewer's help to clarify this very important issue. As seen in Figure 1d and explained in the legend, the lifetime, as well as the emissions were calculated in monthly timesteps.

However, we admit this is not clear in the text, and therefore we have tried to clarify it further there. Some examples of our corrections are in section 2.3 (second paragraph, see Track Changes), Section 3 (first paragraph, see Track Changes), section 3.2 (first paragraph, see Track Changes). As we show in Figure 1d, the temporal trends of ammonia's reactants are considered and appear to have an effect on the lifetime, which varies from 10.3 to 12.2 hours.

2/ A comprehensive overview about the existing literature is missing. For example, result for SO₂ changes in Figure S2 is not in agreement with Krotkov et al., 2016, ACP, showing strong decrease of SO₂ between 2005 and 2015 at least over Eastern US and over Eastern Europe. Also, different publications have shown NH₃ peak in spring over northwestern European countries, not seen here. At least, discrepancies with previous studies should be discussed. These features could be explained by the choice of the authors to analyze their results for Europe or for the US as a whole. An analysis done for the hot-spot regions, of interest, where the emissions are high in Figure 4 may help the analysis.

Response: The legend of SO₂ explains that these are not results from our model/set-up, but assimilated data from NASA's OMI (Ozone Monitoring Instrument) and MERRA2 (Modern-Era Retrospective Analysis for Research and Applications, Version 2). This is also explained in the manuscript (section 3.2, third paragraph, see Track Changes).

About the seasonal variability of the NH₃ emissions, we agree with the reviewer that the spring peaks over northwestern European countries are not seen, because of our choice on the presentation of these results. Since we conduct a global study, we have chosen to study continental emissions rather than focusing only on hot-spot regions. The reason why we did this is because the aim of the paper is not to study the hot-spot emissions of NH₃ as seen from IASI. This has been highlighted already by Van Damme et al. Nature paper (see reference list of the manuscript). We focus on how the prescribed emissions retrieved from IASI can improve modelled concentrations and if models need higher emissions to capture measured concentrations. As a response to if our results are consistent with those of northwestern European countries highlighted in other papers, we plot seasonal emissions of NH₃ for all years, as in Figure 4 of the manuscript (see Fig. R1.1 below).

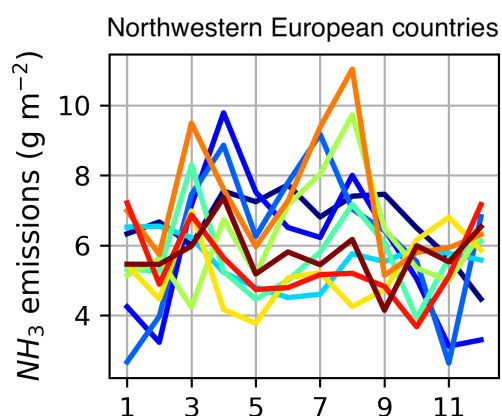


Fig. R1.1: Seasonal emissions of NH₃ in northwestern European countries.

Except for years 2013 and 2015 that peak in summertime, all other years peaked in spring, which is in agreement with the reported hot-spot emissions in northwestern Europe.

3/ The impact of the abundance of sulfuric acid on NH₃ columns is detailed, but not the impact of the abundance of nitric acid. Is this impact considered negligible compared to those of sulfuric acids? This should be discussed. The same Figure S2 for NO₂ columns and nitrate concentrations may help analyzing the results.

Response: We agree with the reviewer. Reactions with nitric acid are not negligible. However, they may have different results in NH₃ concentrations depending on the physicochemical parameters as we explain in the text (neutralization or production of NH₃). We have retrieved NO₂ from OMI, in consistency with SO₂, which we now present in Figure 2 of the manuscript and discuss in the text (section 3.2, circa p. 320-340).

Specific comments:

line 87: a comma is missing before "the Tropospheric Emission Spectrometer"

Response: Corrected (see Track Changes, circa L.87).

line 90-95: a verb is missing in this sentence

Response: Corrected (see Track Changes, circa L.91).

line 96-97: Note that Kuenen and Dore, [2019] estimated the uncertainties linked to the agricultural sector at about 100-300% at the European and an- nual scale.

<https://www.eea.europa.eu/publications/emep-eea-guidebook-2019/part-a-general-guidance-chapters/5-uncertainties/view>

Response: We have added this useful information in the manuscript (see Track Changes, circa L.98).

line 98-102 : What is the differences between the different IASI products? The terms NE, VD0.5 and VDgrlf are not intuitive and are not explained at this stage.

Response: In principle, we agree with the reviewer here. However, we cannot add methodological details in the Introduction, and we'd rather prefer to leave only the names of the different datasets used in the analysis. Further down in the Methods section, we explain in detail what each name refers to and how the results were obtained. We have added a sentence explaining this in circa L.106 (see Track Changes).

line 105: please add references of studies using this state-of-the-art inventory.

Response: The sentence we have added in circa L.106 (see Track Changes) refers to all emission datasets used in the present study including the state-of-the-art emissions from ECLIPSE-GFED4-GEIA and EDGAR-GFED4.

Line 124: could a difference of $2\% \pm 24\%$ just due to the use of particular vertical profiles be interpreted as "small uncertainties"?

Response: We are not sure if we can judge the reported by Van Damme et al. (2018) values on uncertainties. However, as it is stated in their paper, the calculation does not refer to just particular vertical profiles, but rather to a global average: "Differences between columns derived with a fixed vertical profile (baseline) and columns derived using variable modelled profiles are of the order of $2\% \pm 24\%$ on a global scale, but may be substantially larger for individual locations linked to regional differences in meteorological mixing and recirculation."

Line 126-151: the description for CrIS gives more information than for IASI. The analysis of the results may be facilitating with the same information for both the instruments. I encourage you to give more information for IASI (total column uncertainties, peak sensitivity, detection limit, etc).

Response: We have added further details on errors and detection limits for IASI ammonia (see Track Changes in section 2.1.1). Though, we have tried to keep the length of the section consistent with this of CrIS and avoid repetitions, since detailed information of the product is published elsewhere (see references within the manuscript).

Line 152, Section 2.2: could you please provide a map of the interpolated IASI observations? As you performed simulations, it would be great to see the comparison between IASI and the CTM.

Response: We have added this plot in the Supplementary Figure 11, which gives an example of how the gridded results of IASI ammonia compares to the raw data. We believe it is more appropriate to show it there.

Line 155: What is the CTM? As the variable lifetime in section 2.3 is based on this CTM, it should be described before. I would have described LMDZ-OR-INCA before section 2.3.

Response: We agree with the reviewer that the structure was awkward. We have moved the presentation of the CTM first in section 2 of the Methodology (see Track Changes section 2).

Line 160: I would refer to IASI ammonia total columns.

Response: Corrected. Please check at circa L. 214 (Track Changes).

Line 188: Please precise the regions where nitric and sulfuric acids are abundant in the text or at least, refer to Figure 2c and to Figure 2d.

Response: At this point, we discuss the method in general and do not refer to our results. We say that the use of a variable lifetime, and not a constant one, will be able to capture any variability caused by the chemical reactions of ammonia in the atmosphere, where and if they occur.

Line 211: Is the variable lifetime from a CTM for the quantification of VDgrlf emissions similar to the one for the quantification of NE emissions? This is not clear.

Response: We appreciate reviewer's help here. Indeed, this is not clear, and we have now corrected this part (see Track Changes at circa L. 266 of section 2.4).

Line 227-239: Has the NH₃ deposition of LMDz-OR-INCA been already evaluated? Is the bi-directional exchange with surfaces taken into account? This is not discussed. If not, how does it impact your NH₃ emissions?

Response: The total deposition of SO_x, (SO₂+SO₄²⁺), NH_x (NH₃+NH₄⁺), and NO_y (NO+NO₂+NO₃+HNO₂+HNO₃+HNO₄+N₂O₅+organic nitrates+particulate NO₃-) have been evaluated (see Hauglustaine et al., 2014, in the manuscript). However, we admit we do not account for a compensation parameterization in the CTM, as highlighted by the reviewer. We only have the emissions on one side, and the dry deposition ion on the other.

Line 253: you do not focus on hotspot regions but on continents as a whole.

Response: This is true; we agree with the reviewer and we have amended the text at this point (see Track Changes in circa L. 276, first paragraph of section 3).

Line 256-271: the different lifetimes of the literature and your results could be highlighted in a Table.

Response: There is a relevant supplementary Table in Van Damme et al. (2018) Nature paper (see reference within the manuscript), which presents literature values for ammonia lifetimes. We point to this table as "The atmospheric lifetimes of ammonia were summarized in Van Damme et al. (2018)." We do not want to be repetitive and put the same Table here. If the reviewer/editor has a different suggestion, we are willing to correct this in a next stage.

Line 276: As Ammonia lifetime depends on the presence of ammonia's reactants (sulfuric and nitric acid), it also depends on NO_x and SO₂ emissions, not only NH₃ emissions. I would have written "(sulfuric and nitric acids, through SO₂ and NO_x emissions)".

Response: We agree with the reviewer. As we have now clarified in the text, NO₂ and SO₂ are precursors of ammonia's atmospheric reactants, hence lifetime is indirectly

linked to their concentrations. We have followed reviewer's suggestion to amend this sentence (see Track Changes in circa L. 376, p.10).

Figure 1: space is missing between the legend and Figure 1c and 1d

Response: We are not sure we understand where the problem is in Figure 1. Both the legend and the figure appear to be fine in our version. We have corrected some space problems in the title of Fig. 1c (reactants of NH₃) that were overplotted by latitudinal values. If the reviewer still thinks there's a space missing somewhere, we could correct it in a next stage of the reviewing process.

Line 287: "which is in the range of the previously reported values". Your results are far from the results from Dammers et al [2019] for example. How do you explain such differences? Could the simulated NH₃ lifetime by CTM be over-estimated?

Response: We cannot judge the values calculated by Dammers et al. [2019]. As we report in circa L. 367-370 "The majority of ammonia lifetimes reported regionally or globally fall within 10 and 24 hours independently of the different approaches (Hauglustaine et al., 2014; Hertel et al., 2012; Möller and Schieferdecker, 1985; Sutton et al., 1993; Whitburn et al., 2016b),...".

Line 296: Please note in the legend of Figure 1b that the average ammonia emissions are calculated from the 10-year IASI observations and precise with which lifetime. I first thought it was the average ammonia emissions from ECLIPSEv5-GFED4-GEIA. Please also verify the legend of Figure S3.

Response: We thank the reviewer here; We have now clarified that the plot refers to the NE emissions (Track Changes at legend of Figure 1). We have also clarified this in the legend of the supplementary Figure S3.

Line 320-321: The sentence "Although column concentrations of both sulfur dioxide and sulfates present strong interannual variability, they do not show significant changes on an annual basis" is not clear. Please rephrase.

Response: We have amended this sentence to be consistent with what the figures show. Please see Track Changes at circa L. 428-432 (p.12).

Line 331: I do not understand why the anomaly is calculated only after 2015. Please explain.

Response: We initially thought to study anomalies after 2015, as our calculated emissions seem to increase after 2015. We agree with the reviewer that changes are already obvious since 2012 and now provide a more complete reasoning supported by relevant references. However, the largest reductions were seen after 2015, in agreement with the emissions of NH₃ that we present here, as seen in the attached Fig. R1.2 and that is why we have chosen to restrict anomalies after 2015. Please see Track Changes at p.11-12.

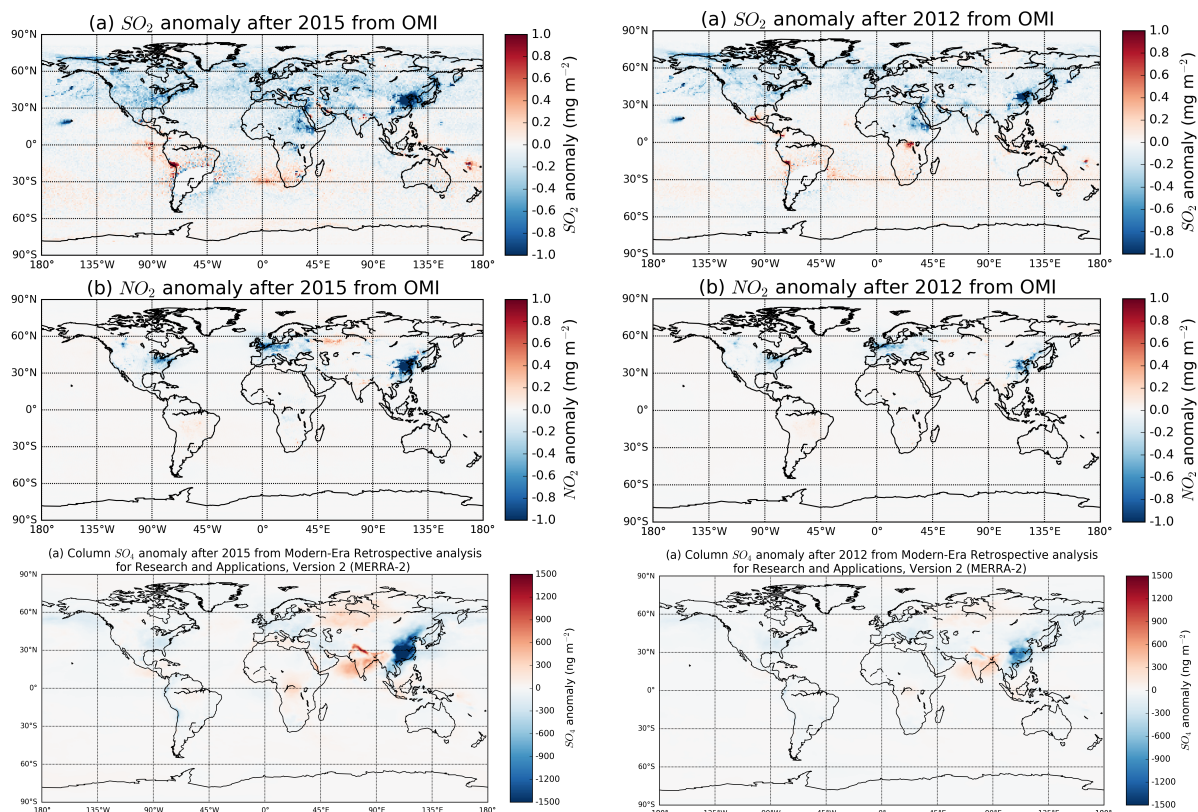


Fig. R1.2: Left column: SO₂, NO₂ and SO₄ anomalies after 2015, as in the present manuscript. Right column: same anomalies calculated after 2012, when the first reductions of these precursors of NH₃ reactants were observed.

Line 334-337: why the NH₃ emissions based on IASI observations could be impacted by changes in SO₂ and NO_x emissions only after 2015? In Lachatre et al., 2019, the study you are citing line 337, the changes in SO₂ at least are seen before 2015. This is also the case in your Figure S2. Please strengthen this discussion.

Response: As we now discuss in L. 418-p.11, although the SO₂ and NO_x reduction is evident since 2012, the largest changes are calculated for the period after 2015, which is in agreement with our suggested NH₃ emissions. This is also evident if we compare anomalies after 2012 with those after 2015 as in the attached Fig.2. Therefore, we present anomalies after 2015. We have tried to explain this in the manuscript (please see Track Changes in p.11-12).

Line 352: please deeply detail why the fact that northern India has been previously identified as a hot-spot region for ammonia explains the differences between the emission datasets.

Response: We believe we do not imply that the fact that N. India has been identified as a hotspot region explains the difference in the emission datasets. We only say that these hotspot emissions in N. India have been highlighted to be due to agricultural activities and we give 2 references to support this. We have now tried to re-write the sentence (see Track Changes at circa L. 476).

Line 335: Please verify the species indices

Response: We have amended this part and the overall discussion in this section as explained in previous comments (see Track Changes at p. 11-12).

Line 356: the ammonia emissions remain mostly constant at the global scale. Is it still true at continental scale?

Response: Yes, it is actually true that no significant continental changes occurred. For example, the ECLIPSE emissions which are based on the GAINS model are produced for 5-year timesteps. What global models assume is usually a linear interpolation to scale the emissions for each of the years in between. For justification, we plot the annual emissions from ECLIPSEv5-GFED4-GEIA and from EDGARv4.3.1-GFED4 in the attached Figs R1.3 and R1.4.

ECLIPSEv5-GFED4-GEIA

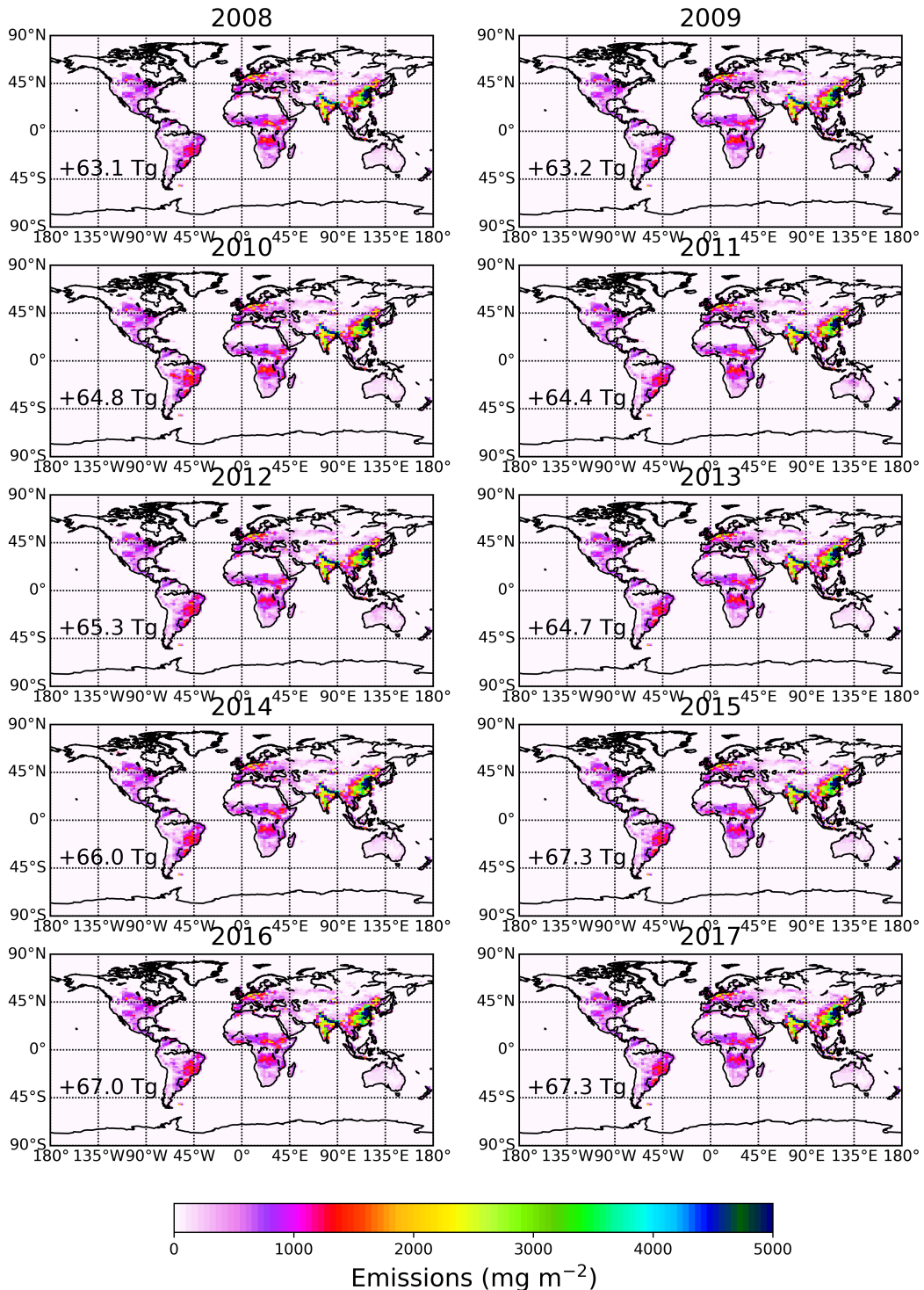


Fig. R1.3: Annual emissions of NH₃ in ECLIPSEv5-GFED4-GEIA.
EDGARv4.3.1-GFED4

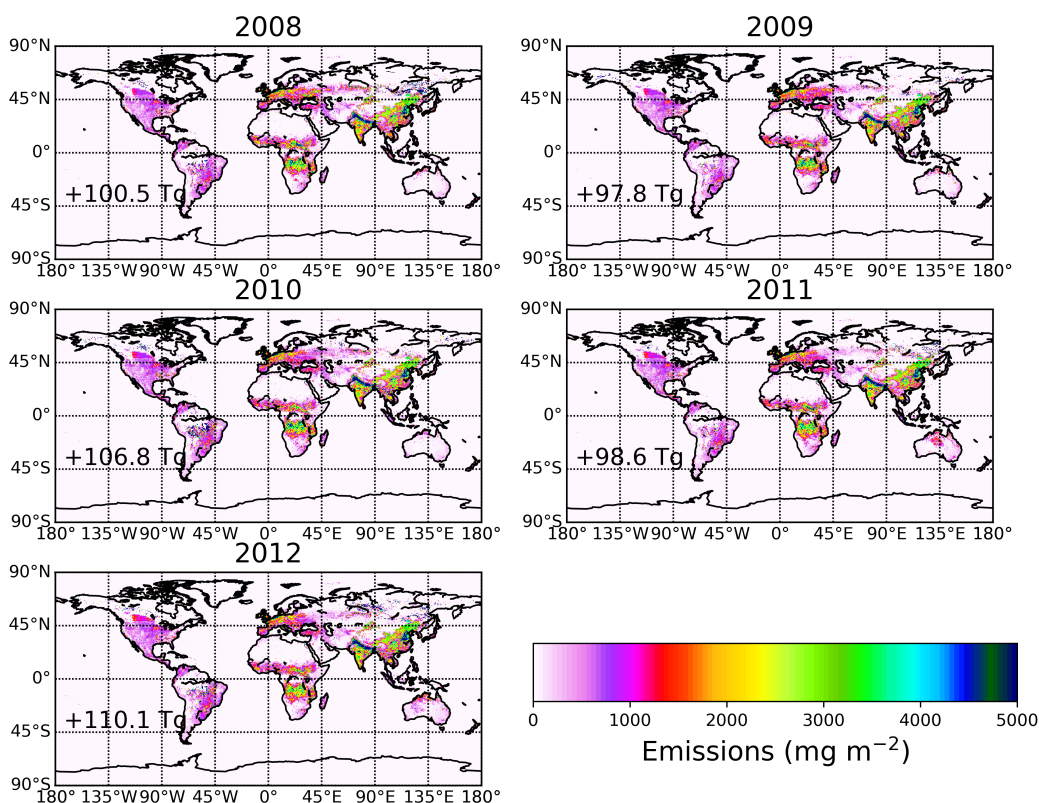


Fig. R1.4: Annual emissions of NH₃ in EDGARv4.3.1-GFED4.

Line 357: “The total calculated ammonia emissions”: which one?

Response: We have amended this sentence (Track Changes at circa L.641-642).

Line 360-363: could you please provide statistics (average and standard deviation) for South American and European emissions as well as for the global budget?

Response: We have amended this part. Numbers have been added everywhere in this paragraph presenting average and sd (see Track Changes at L.491-496, p. 13).

Line 363-364: “Based upon IASI retrievals, Liu et al. (2019) showed an increase of surface NH₃ concentrations trend of more than 0.2 μgNm⁻³yr⁻¹”: I do not understand the link with the previous sentence.

Response: We consent with this comment and we have removed this sentence thanks to the reviewer (see Track Changes at circa L.496, p. 13).

Line 365: “Ammonia emissions derived over China in this work are among the highest worldwide (Figure S1)”: is this already the case in the EDGAR and EGG bottom-up inventories or is this a new feature?

Response: We have made clear that by saying “in this work” we mean the emissions highlighted as NE (see Track Changes at circa L.496, p. 13).

Line 370: please precise “The comparison of the annual ammonia NE emissions. . .” In general, you should specify the inventory or the sensitivity test you are referring to, it would help for the reading and for the understanding of the study.

Response: The reviewer is again right here. We have modified the sentence as follows: “The comparison of the annual ammonia emissions in the NE dataset to the ...” (see Track Changes, L.509, p.14).

Line 377: I would add “in these regions” at the end of the sentence. Indeed, the impact of the different lifetimes seems to be slight over the other regions of the world.

Response: Corrected as suggested by the reviewer (see Track Changes, L.517, p.14)

Line 385-386: is this contradictory with the sentence “European emissions are practically identical in all datasets” in line 361?

Response: We have modified the sentence as follows “... in all datasets except EGG ...” (see Track Changes, L.493, p.13).

Line 460: consist in?

Response: We have corrected as suggested (see Track Changes, L.601, p.17).

Line 461-470: The description of the different inventories and of the different performed simulations should occur before in the text. I would have placed this paragraph at the end of the introduction.

Response: The sequence of the paper is (a) proof that modelled lifetimes are realistic, (b) presentations of the different emission inventories for NH₃ based on different methodologies, (c) comparison with state of the art datasets (ECLIPSE-GFED-GEIA, EDGAR-GFED) that are frequently used to simulate NH₃ concentrations in global models.

Then, we need to prove that the emissions presented in the paper produced more realistic modelled concentrations, and for this reason, we simulate NH₃ using each of the different emissions and compare model concentrations with surface measurements and satellite data. We explain all these in an introductory paragraph in discussions. However, we agree with the reviewer and have moved the part that explains what the EGG emissions refer to into the place that appear for the first time. Instead, we use abbreviations everywhere in this paragraph.

Figure 4: you should number the different graphs. It would be easier to reference them in the text. Please better describe the NH₃ emission dataset in the legend.

Response: We do not really use the numbering in any part of the text when refer to this figure. This is mainly done because each graph placed in any row shows exactly the same thing for different continental regions. We do not think this is necessary (since it's not used) and if the reviewer/editor insists, we may do so in a next step.

Line 532: there is an empty bracket.

Response: Bracket has now been removed (see Track Changes, p.19).

Section 4.2: Does the evaluation against CrIS done at the global scale? It is not specified. If it is the case, it is not comparable with the surface evaluation done at the regional scale. It would be very interested to do it also at regional scale for the analysis, as in Figure 5, 6 and 7 and particularly over hot-spots as explained in the major comments.

Response: Yes, the comparison with CrIS NH₃ refers to global data, which we now specify in L. 677-678. As we already answered in a previous comment, an evaluation

of IASI ammonia for several hotspot regions has been done in Van Damme et al. (2018) Nature paper. What we do here is to use IASI NH₃ to produce emissions and see if a model that participates in CMIP and IPCC simulations can improve its performance, also giving these emissions to be used by anyone interested. We evaluate the modelled concentrations against ground measurements that we trust more, in general for N. America, Europe and Southeastern Asia. As a supplement we compare with another global product (CrIS), to prove that concentrations are better reproduced, not only in N. America, Europe and Southeastern Asia, but in a global scale.

Line 599: the word “already” is misplaced in the sentence.

Response: “already” should be “although” in this sentence. We thank the reviewer for pointing this out. We have amended the sentence (see Track Changes, L.736, p.21).

Figure 9: the colors of the scale should be changed: when the uncertainty is high, the borders on the map are not clearly visible.

Response: We have used another colormap as suggested by the reviewer, in order to have visible coastlines (see manuscript with Track Changes).

Line 612: what are the regions with “changing balance between nitrate and sulfate abundances”? Please detail in the text.

Response: We have amended the sentence to make a more concrete statement as suggested (see Track Changes as L. 751-753, p. 21).

Anonymous Referee #2

Received and published: 27 November 2020

Overall, the paper is well written and provides new information to the literature on global NH₃, which has not been well characterized previously. The paper is rather long and could condense it down to a tighter paper that is more focused on key results and conclusions.

Response: We appreciate reviewer's comments and his willingness to improve this manuscript. We have made all the changes requested by the 2 reviewers and we are willing to further work to shorten the manuscript, if additional detailed comments are to be requested.

Comparing model predictions at the coarse level presented here (2.5 degrees or 250 km) to ground monitors and discussing "hotspots" may not well represent the spatially variable nature of NH₃ emissions. Averages over these large cells could misrepresent key features of NH₃ distributions. However, the spatial resolution in Figure 4 appears to be finer than 2.5 x 1.3 degree. Was a particular plotting technique used to show the NH₃ levels that might be making gradient interpolations or is the data in Figure 4 actually 2.5 x 1.3 degree resolution?

Response: We acknowledge reviewer's observation here and we admit this was misleading. We have now clarified in section 2.3 (see Track Changes at p.7-8). What we have done was to process the IASI column concentration measurements onto a grid of 0.5°×0.5° using the IDW method that we describe in section 2.3. Then, since the resolution of the CTM model that we used bilinear interpolation classic method to convert to the model resolution (2.5°×1.3°).

The authors estimated emission fluxes using a lifetime parameter from the CTM. Was there some reason a traditional assimilation approach (e.g., like Alvarado is doing) was not included in this assessment? The authors should consider a comparison of the column predictions of the CTM simulation using the estimated emissions back to the IASI measurements. If the lifetime approach is accurate, the CTM should accurately predict the IASI columns when using the scaled emissions. If this was done it is not clear from the text. Further, it did not seem like the seasonal NH₃ lifetime estimated by the CTM provided a substantively different result than the 0.5VD constant assumption.

Response: There was not special reason for not using a classic assimilation method here. Our idea was to try to calculate emissions from IASI column NH₃ measurements. For this, we needed a metric of the lifetime of NH₃. We used a constant lifetime of 0.5 d everywhere, as well as a gridded one, calculated from a model, which we thought it is more realistic, as ammonia cannot have the same lifetime everywhere (see section 3.1). Finally, we wanted to see if the calculated emissions have a significant impact on surface concentrations. For this, we compare with measurements from EMEP, EANET and AMoN.

The goal of this paper is not to validate the CTM against IASI column ammonia. However, an example of how the column NH₃ in the model compares to IASI column NH₃ is now given in Supplementary Figure S11 (of the manuscript). The model is continuously validated by the LSCE group (see relevant papers here:

https://www.lsce.ipsl.fr/en/Phoce/Vie_des_labos/Ast/ast_groupe.php?id_groupe=94&voir=publis). We rather want to prove that for very short-lived species such as NH₃, a simple approach like the one we describe in section 2 is enough to constrain

the main source of NH₃ in the atmosphere, a chemical species that is difficult to be quantified with classic inverse modelling approaches, due to its heterogeneous chemistry. The goals of this manuscript are explained in detail in the last paragraph of the introduction.

The reviewer states that “, it did not seem like the seasonal NH₃ lifetime estimated by the CTM provided a substantively different result than the 0.5VD constant assumption”. We only show the lifetime calculated by the CTM in Figure 1d (of the manuscript), which basically shows values between 10 – 12.5 hours, whereas in VD0.5 a constant lifetime of 12 hours (0.5 d) was used everywhere. The difference in the emissions using a variable versus a constant lifetime for NH₃ are shown in Figure 3 (of the manuscript) and they are as high as 29.4 Tg/y (on average), or 15% different, which we do think it is substantially different; both in absolute numbers, but also in the spatial distribution of the emissions. The impact on the surface concentrations against observations is shown in both as time-series plots in the Supplements and as scatterplots in the main text. The IASI-constrained emissions, at least in the North America and Southeastern Asia, capture realistically atmospheric concentrations (see linear scale in x- and y-axes).

Ammonia has a strong diurnal profile. Does the assumption for diel profile impact any of the results presented in this paper or does the diurnal nature of NH₃ emissions have no impact on these products?

Response: Indeed, NH₃ has a strong diurnal cycle, and the CTM uses a means to account for a diurnal cycle. However, we have not assessed how the diurnal cycle in the present setup affects the results. The reason is that, although IASI NH₃ are measured twice a day, only morning measurements were used in the present study, due to the larger thermal conditions that lead to smaller uncertainties. Accordingly, we have used daily model outputs for concentrations and monthly mean lifetimes from the model. In addition, all measurements used here to evaluate modelled concentrations have a temporal resolution of 1 or 2 weeks. Therefore, no further effort to deal with the diurnal cycle of NH₃ was made and rather assumed that it should not affect much our results. Of course, we have to admit that a bias in the overall assessment could be realistic, although no data to prove this were available.

When taking a closer look at Figure 6, is it surprising that VD0.5, NE, and VDgrid emissions used in a model result in very few model estimations of ammonia below 0.5 and ECG rarely has a prediction above 0.5. Some of the calculated performance metrics may suggest “good” model performance but the shape of the model-observed NH₃ in Figure 6 shows some features that suggest they many of these approaches can not replicate the range of NH₃ levels measured.

Response: We rather think this is normal. As one can read in section 3.4, “North American annual ammonia emissions over the 10-year period were averaged 1.1 ± 0.1 Tg yr⁻¹ (average \pm sd). These values are over two orders of magnitude higher than those in EGG (0.062 ± 0.0013 Tg yr⁻¹). Note that his estimate is three times lower than those reported in VD0.5 (3.1 Tg yr⁻¹) or in VDgrlf (3.4 ± 0.5 Tg yr⁻¹).” Therefore, we see smaller MFB values (=0.32) in Figure 6 (of the manuscript) than those of VD0.5 (=0.52) and VDgrlf (=0.54) and much higher than those in EGG (= -0.28). Another view of the modelled-observation mismatches can be seen in supplementary Figures S7-S9.

Please provide some more clarity on the vertical profile used for NH₃ for IASI retrievals. Is this constant and not variable with changes in altitude? Does the vertical profile conform to profiles measured as part of aircraft measurement campaigns and seem realistic?

Response: We have not used any vertical profile for IASI NH₃. As we explain in detail in p.7-L.316 “IASI total column ammonia measurements were interpolated onto ...” a grid with the method described in section 2.3. Then, a box-model was used to calculate gridded emissions of NH₃, as described in section 2.4 (L. 368-370, p. 8): “It takes into account the gridded column concentrations of ammonia that were calculated with the IDW interpolation method and all the potential removal processes of ammonia occurring in a hypothetical atmospheric box...”.

Line 581: What are large sources of anthropogenic NH₃ in central USA?

Response: We explain this, two paragraphs before this point. Please check manuscript with Track Changes (l.599-618): “First, a small region in Colorado, Central US, which is the location of a large agricultural region that traditionally releases large ammonia emissions...”. Then, we continue explaining main sources in Central US “is the state of Iowa (home to more than 20 million swine, 54 million chickens, and 4 million cattle), northern Texas and Kansas (beef cattle) ...”. We think it is a repetition to mention again and again something that has been explained a few lines before.

Figure 8 is very hard to interpret. The authors should consider alternative colors or another way to present these results.

Response: We have chosen to use the Gaussian kernel density estimation (KDE) method due to the large amount of data that we had to process, and we thought we should avoid overplotting. Another way to show the improvement of the results would be simple scatterplots that present annual data from all 4 simulations (Fig. R2.1). The reviewer/editor can possibly decide which one shows better. We would rather prefer the KDE method.

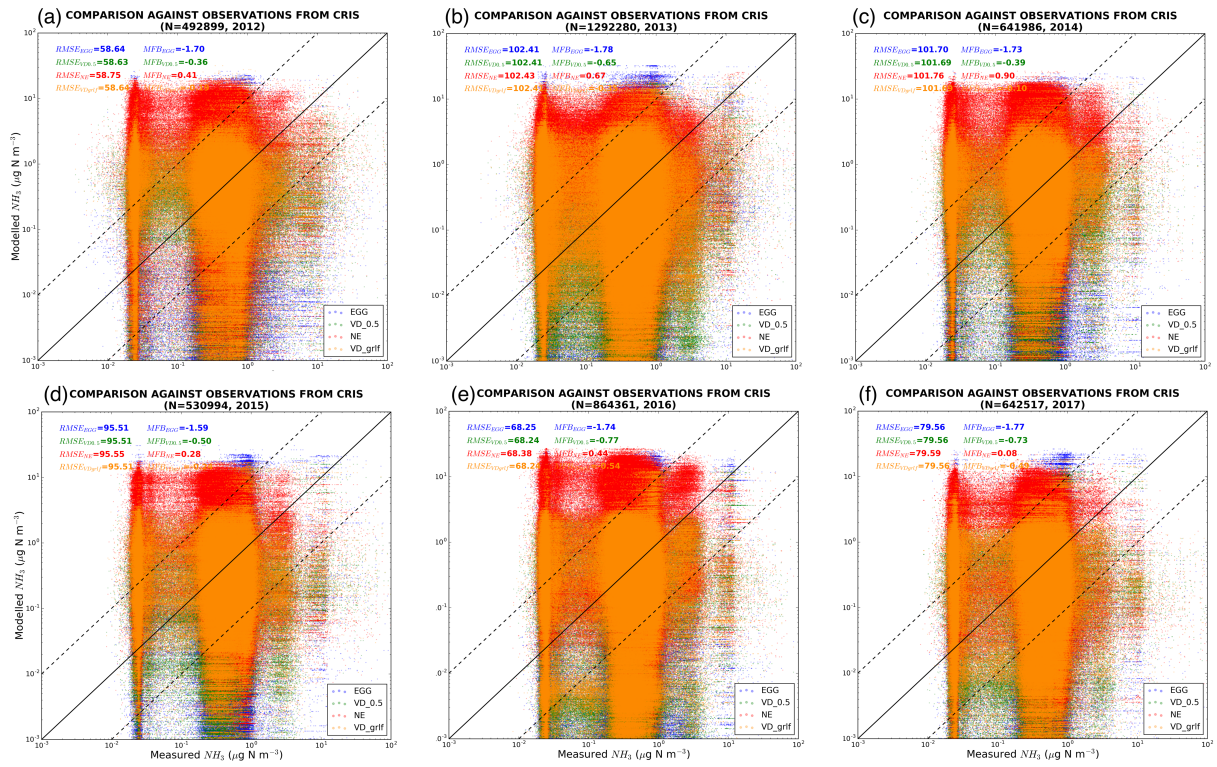


Fig. R2.1: Annual scatterplots of modelled versus CrIS NH_3 surface concentrations from the relevant four simulations using emissions from EGG, VD0.5, NE and VDgrlf.

1 **10–year satellite–constrained fluxes of ammonia improve**
2 **performance of chemistry transport models**

3

4 **Nikolaos Evangeliou^{1,*}, Yves Balkanski², Sabine Eckhardt¹, Anne Cozic², Martin**
5 **Van Damme³, Pierre-François Coheur³, Lieven Clarisse³, Mark W. Shephard⁴,**
6 **Karen E. Cady-Pereira⁵, Didier Hauglustaine²**

7

8 ¹Norwegian Institute for Air Research (NILU), Department of Atmospheric and Climate
9 Research (ATMOS), Kjeller, Norway.

10 ²Laboratoire des Sciences du Climat et de l'Environnement (LSCE), CEA-CNRS-UVSQ,
11 91191, Gif-sur-Yvette, France.

12 ³Université libre de Bruxelles (ULB), Spectroscopy, Quantum Chemistry and Atmospheric
13 Remote Sensing (SQUARES), Brussels, Belgium.

14 ⁴Environment and Climate Change Canada, Toronto, Ontario M3H 5T4, Canada.

15 ⁵Atmospheric and Environmental Research, Inc., Lexington, MA, USA.

16

17 * Corresponding author: N. Evangeliou (Nikolaos.Evangeliou@nilu.no)

18

19 **Abstract**

20 In recent years, ammonia emissions have been continuously increasing being almost four
21 times higher than in the 20th century. Although an important species as its use as a fertilized
22 sustains human living, ammonia has major consequences both for humans and the environment,
23 because of its reactive gas phase chemistry that makes it easily convertible to particles. Despite
24 its pronounced importance, yet, ammonia emissions are highly uncertain in most emission
25 inventories. However, the great development of satellite remote sensing nowadays provides the
26 opportunity for more targeting research in constraining ammonia emissions. Here, we used
27 satellite measurements to calculate global ammonia emissions over the period 2008–2017.
28 Then, the calculated ammonia emissions were fed to a chemistry transport model and ammonia
29 concentrations were simulated for the period 2008–2017.

30 The simulated concentrations of ammonia were compared with ground measurements
31 from Europe, North America and Southeastern Asia, as well as with satellite measurements.
32 The satellite-constrained ammonia emissions represent global concentrations more accurately
33 than state-of-the-art emissions, which underestimate ammonia with a factor of two. Calculated
34 fluxes in the North China Plain were [seen more](#) increased after 2015, not due to emission
35 changes, but due to changes in sulfate emissions that resulted in less ammonia neutralization
36 and hence in larger atmospheric loads. Emissions over Europe were also twice as much as those
37 in traditional datasets with dominant sources to be industrial and agricultural applications. Four
38 hot-spot regions of high ammonia emissions were seen in North America characterized by large
39 agricultural activity (Colorado), animal breeding (Iowa, northern Texas and Kansas), animal
40 farms (Salt Lake, Cache, and Utah) and animal breeding and agricultural practices (California).
41 South America is dominated by ammonia emissions from biomass burning, which cause a
42 strong seasonality. In Southeastern Asia, ammonia emissions from fertilizer plants in China,
43 Pakistan, India and Indonesia are the most important, while a strong seasonality was observed
44 with a spring and late summer peak due to rice and wheat cultivation. Modelled concentrations
45 from the satellite-constrained ammonia emissions are overestimated in Eastern Europe, where
46 state-of-the-art emissions capture observations better. Measurements of ammonia
47 concentrations in North America were better reproduced with satellite-constrained emissions,
48 while all emissions generally underestimate station concentrations in Southeastern Asia. The
49 calculated ammonia emissions also reproduce global CrIS (Cross-track Infrared Sounder)
50 observations more effectively.

51

52 **1 Introduction**

53 Ammonia (NH₃) has received a lot of attention nowadays due to its major implications
54 for the population and the environment (Erisman, 2004; Erisman et al., 2007). These include
55 eutrophication of semi-natural ecosystems and acidification of soils (Stevens et al., 2010),
56 secondary formation of particulate matter in the atmosphere (Anderson et al., 2003), and
57 alteration of the global greenhouse balance (De Vries et al., 2011). More specifically in the
58 troposphere, ammonia reacts with the abundant sulfuric and nitric acids (Malm, 2004)
59 contributing 30 % to 50 % of the total aerosol mass of PM_{2.5} and PM₁₀ (Anderson et al., 2003).
60 Ammonium aerosols are therefore a very important component in regional and global aerosols
61 processes (Xu and Penner, 2012) also having significant implications for human health (Aneja
62 et al., 2009). Ammonia alters human health indirectly mainly through formation of PM_{2.5} (Gu
63 et al., 2014) that penetrate the human respiratory systems and deposit in the lungs and alveolar
64 regions (Pope III et al., 2002) causing premature mortality (Lelieveld et al., 2015). As regards
65 to the climate impact, the same ammonium aerosol particles affect Earth's radiative balance,
66 both directly by scattering incoming radiation (Henze et al., 2012) and indirectly as cloud
67 condensation nuclei (Abbatt et al., 2006). They may also cause visibility problems and
68 contribute to haze effect due to secondary PM formation.

69 Sources of ammonia include wild animals (Sutton et al., 2000), ammonia-containing
70 watersheds (Sørensen et al., 2003), traffic (Kean et al., 2009), sewage systems (Reche et al.,
71 2012), humans (Sutton et al., 2000), biomass burning (Sutton et al., 2008) and domestic coal
72 combustion (Fowler et al., 2004), volcanic eruptions (Sutton et al., 2008) and agriculture
73 (Erisman et al., 2007). The latter is responsible for the majority of ammonia global atmospheric
74 emissions. Specifically, in the United States and Europe about 80% of all emissions is related
75 to agriculture (Leip et al., 2015). Emissions have increased considerably since pre-industrial
76 times and are unlikely to decrease due to the growing demand for food and feed (Aneja et al.,
77 2008).

78 The growing attention in ammonia levels has enabled many monitoring actions in Europe
79 (European Monitoring and Evaluation Programme, EMEP), in Southeastern Asia (East Asia
80 acid deposition NETwork) and in the North America (Ammonia Monitoring Network in the
81 US, AMoN-US; National Air Pollution Surveillance Program (NAPS) sites in Canada) to
82 record surface concentrations of ammonia continuously. Recently, several satellite products
83 have been also developed in an effort to identify global levels of ammonia considering that the

84 relatively sparse existing monitoring network has an insufficient coverage for this purpose.
85 These are derived from satellite sounders as the Infrared Atmospheric Sounding Interferometer
86 (IASI) (Van Damme et al., 2017), the Atmospheric Infrared Sounder (AIRS) (Warner et al.,
87 2017), the Cross-track Infrared Sounder (CrIS) (Shephard and Cady-Pereira, 2015), the
88 Tropospheric Emission Spectrometer (TES) (Shephard et al., 2015), and Greenhouse Gases
89 Observing Satellite (Someya et al., 2020). Both IASI and CrIS ammonia products are being
90 continuously compared and evaluated against other observations and products. Relevant
91 analyses include comparison against column-integrated levels measured by Fourier transform
92 infrared spectroscopy (FTIR) (Dammers et al., 2016, 2017), ground-based measurements (Van
93 Damme et al., 2015; Kharol et al., 2018), bottom-up emissions (Van Damme et al., 2018;
94 Dammers et al., 2019) and atmospheric chemistry transport models (CTMs) (Shephard et al.,
95 2020; Whitburn et al., 2016a).

96 Despite its importance, ammonia is a poorly quantified trace gas, with uncertainties over
97 50% on the global emission budget and even higher on temporal and local scales (Dentener and
98 Crutzen, 1994; Faulkner and Shaw, 2008; Reis et al., 2009) and up to 300% for the agricultural
99 sector in Europe (European Environment Agency, 2019). In the present paper, we grid 10 years
100 (2008–2017) of satellite measurements of ammonia retrieved from IASI to calculate monthly
101 surface emissions (hereafter named NE) (see section 2). The same is done using the gridded
102 IASI ammonia column concentrations from Van Damme et al. (2018) (named as VD0.5 and
103 VDgrlf) (see section 2). The three different emission inventories together with a state-of-the-
104 art one, which is more often used by models (named as EGG), are then imported in a CTM to
105 simulate ammonia for the same 10-year period. More details of the different emissions used
106 here are shown in sections 2.4 and 2.1. Finally, an evaluation of simulated surface
107 concentrations against ground-based measurements from different monitoring stations and
108 satellite products allow to quantify the improvements in ammonia emissions.

109 2 Methods

110 2.1 LMDz-OR-INCA chemistry transport model

111 The Eulerian global CTM LMDz-OR-INCA was used to calculate ammonia lifetime, as
112 well as to simulate ammonia concentrations from the emission fluxes calculated from IASI
113 satellite products. The model couples the LMDz (Laboratoire de Météorologie Dynamique)
114 General Circulation Model (GCM) (Hourdin et al., 2006) with the INCA (INteraction with
115 Chemistry and Aerosols) model (Folberth et al., 2006; Hauglustaine et al., 2004) and with the

Deleted:

Deleted: For example,

Moved (insertion) [1]

118 land surface dynamical vegetation model ORCHIDEE (ORganizing Carbon and Hydrology In
119 Dynamic Ecosystems) (Krinner et al., 2005). In the present configuration, the model has a
120 horizontal resolution of 2.5°×1.3°, the vertical dimension is divided into 39 hybrid vertical
121 levels extending to the stratosphere. Large-scale advection of tracers is calculated from a
122 monotonic finite-volume second-order scheme (Hourdin and Armengaud, 1999), deep
123 convection is parameterized according to the scheme of Emanuel, (1991), while turbulent
124 mixing in the planetary boundary layer (PBL) is based on a local second-order closure
125 formalism. More information and a detailed evaluation of the GCM can be found in Hourdin et
126 al. (2006).

127 The model simulates atmospheric transport of natural and anthropogenic aerosols
128 recording both the number and the mass of aerosols. The aerosol size distribution is represented
129 using a modal approach that consists of the superposition of 5 log-normal modes that represent
130 both the size spectrum and whether the aerosol is soluble or insoluble (Schulz, 2007). The
131 aerosols are treated in three particle modes, sub-micronic (diameter < 1 µm) corresponding to
132 the accumulation mode, micronic (diameter 1–10 µm) corresponding to coarse particles, and
133 super-micronic or super coarse particles (diameter > 10 µm). LMDz-OR-INCA accounts for
134 emissions, transport (resolved and sub-grid scale), and dry and wet (in-cloud/below-cloud
135 scavenging) deposition of chemical species and aerosols interactively. LMDz-OR-INCA
136 includes a full chemical scheme for the ammonia cycle and nitrate particle formation, as well
137 as a state-of-the-art CH₄/NO_x/CO/NMHC/O₃ tropospheric photochemistry. Further details
138 about specific reactions, reaction rates and other information entering into the description of
139 the ammonia cycle can be found in Hauglustaine et al. (2014).

140 The global transport of ammonia was simulated from 2007 to 2017 (2007 was the spin-
141 up period) by nudging the winds of the 6-hourly ERA Interim Reanalysis data (Dee et al., 2011)
142 with a relaxation time of 10 days (Hourdin et al., 2006). For the calculation of ammonia's
143 lifetime, the model ran with traditional emissions for anthropogenic, biomass burning and
144 oceanic emission sources using emissions from ECLIPSEv5 (Evaluating the CLimate and Air
145 Quality ImPacts of Short-livEd Pollutants), GFED4 (Global Fire Emission Dataset) and GEIA
146 (Global Emissions InitiAtive) (hereafter called EGG) (Bouwman et al., 1997; Giglio et al.,
147 2013; Klimont et al., 2017).

Deleted: -

Deleted: -

Deleted:

Deleted:

152 **2.2 Satellite ammonia**

153 **2.2.1 IASI ammonia**

154 The Infrared Atmospheric Sounding Interferometer (IASI) onboard the MetOp-A satellite
155 measures Earth's infrared radiation twice a day in a spectral range of 645–2,760 cm⁻¹ with an
156 elliptical footprint with a diameter of 12 km at nadir (Clerbaux et al., 2009). Due to the larger
157 thermal conditions that lead to smaller uncertainties, only morning data were used in the present
158 assessment (Clarisse et al., 2010). Van Damme et al. (2018) reported limited impact of the IASI
159 overpasses of 4%±8% on ammonia. The 10-year dataset used here is ANNI-NH3-v2.1R-I
160 product (Van Damme et al., 2017) and relies on ERA-Interim ECMWF meteorological input
161 data (Dee et al., 2011). The Artificial Neural Network for IASI (ANNI) algorithm converts the
162 hyperspectral range index to a column-integrated NH₃ value (Whitburn et al., 2016a). The
163 latter relies on the fact that the indices can be converted to a column by taking into account the
164 spectral sensitivity to the ammonia abundance in the observed scene. The hyperspectral range
165 indexes are derived from linear retrievals using a constant gain matrix which includes a
166 generalized error covariance matrix (Van Damme et al., 2014b; Whitburn et al., 2016a). The
167 dataset also provides cloud coverage for each measurement (August et al., 2012). Only
168 measurements with a cloud fraction below 10% were processed in consistency with Van
169 Damme et al. (2018). Cloud coverage was not provided for all measurements until March 2010
170 resulting in smaller data availability before that date. Van Damme et al. (2014a) reported that
171 IASI better measures ammonia in spring and summer months, due to the strong dependence on
172 thermal contrast (error below 50%). For an individual observation, an IASI-retrieved column
173 is considered detectable when the vertical column density exceeds 9.68×10¹⁵ molecules cm⁻²
174 (surface concentration > 1.74 μg m⁻³) at a thermal contrast of 20 K, while the vertical column
175 density should be larger than 1.69×10¹⁶ molecules cm⁻² (3.05 μg m⁻³) at 10 K (Van Damme et
176 al., 2014a). Although the retrieval algorithm uses a fixed vertical profile, extended validation
177 of the resulting dataset has verified small uncertainties (Van Damme et al., 2015, 2018;
178 Dammers et al., 2016; Whitburn et al., 2016b). For instance, Van Damme et al. (2018) reported
179 a difference of 2%±24% (global average) in column-integrated ammonia using different
180 vertical profiles in the retrieval algorithm.

181 **2.2.2 CrIS ammonia**

182 The Cross-Track Infrared Sounder (CrIS) was first launched on the NASA Suomi
183 National Polar-orbiting Partnership (S-NPP) satellite on 28 October 2011 in a sun-synchronous
184 low Earth orbit. The CrIS sensor provides soundings of the atmosphere with a spectral

Deleted: (at nadir circular

Deleted:)

Formatted: Norwegian Bokmål

Formatted: Norwegian Bokmål

Formatted: Norwegian Bokmål

Field Code Changed

Formatted: Norwegian Bokmål

Deleted:

Deleted: (

Deleted: ,

Formatted: Superscript

Formatted: Superscript

Formatted: Superscript

Formatted: Superscript

Formatted: Superscript

Field Code Changed

Deleted:

191 resolution of 0.625 cm^{-1} (Shephard et al., 2015). One of the main advantages of CrIS is its
192 improved vertical sensitivity of ammonia closer to the surface due to the low spectral noise of
193 $\sim 0.04\text{K}$ at 280K in the NH_3 spectral region (Zavalyov et al., 2013) and the early afternoon
194 overpass that typically coincides with high thermal contrast, which is optimal for thermal
195 infrared sensitivity. The CrIS Fast Physical Retrieval (CFPR) (Shephard and Cady-Pereira,
196 2015) retrieves an ammonia profile (14 levels) using a physics-based optimal estimation
197 retrieval, which also provides the vertical sensitivity (averaging kernels) and an estimate of the
198 retrieval errors (error covariance matrices) for each measurement. As peak sensitivity is
199 typically in the boundary layer between 900 and 700 hPa (~ 1 to 3 km) (Shephard et al., 2020),
200 the surface and total column concentrations are both highly correlated with the retrieved levels
201 in the boundary layer. Shephard et al. (2020) reports estimated total column random
202 measurement errors of 10–15%, with estimated total random errors of $\sim 30\%$. The individual
203 profile retrieval levels have estimated random measurement errors of ~ 10 to 30% , with
204 estimated total random errors increasing to 60 to 100% due to the limited vertical resolution.
205 These vertical sensitivity and error output parameters are also useful for using CrIS
206 observations in applications (e.g. data fusion, data assimilation; model-based emission
207 inversions (e.g., Cao et al., 2020; Li et al., 2019) as a satellite observational operator can be
208 generated in a robust manner. The detection limit of CrIS measurements has been calculated
209 down to $0.3\text{--}0.5 \text{ ppbv}$ (Shephard et al., 2020). CrIS ammonia has been evaluated against other
210 observations over North America with the Ammonia Monitoring Network (AMoN) (Kharol et
211 al., 2018) and against ground-based Fourier transform infrared (FTIR) spectroscopy
212 observations (Dammers et al., 2017) showing small differences and high correlations.

213 2.3 Inverse Distance Weighting (IDW) interpolation

214 To process large amounts of measurements in a 2-dimensional grid of high resolution,
215 oversampling methods (Streets et al., 2013) can be used (Van Damme et al., 2018). However,
216 considering that the resolution of the CTM is $2.5^\circ \times 1.3^\circ$ (see section 2.4), there is no need to
217 process the measurements on such a high-resolution grid and therefore an interpolation method
218 was used. The method has been extensively used after the Chernobyl accident in 1986 to
219 process more than 500 thousand deposition measurements over Europe (De Cort et al., 1998;
220 Evangeliou et al., 2016).

221 IASI total column ammonia measurements were interpolated onto a grid of $0.5^\circ \times 0.5^\circ$
222 using a modified Inverse Distance Weighting (IDW) algorithm described by (Renka, 1988).

- Deleted: as
- Deleted: 2
- Deleted: 1.3
- Formatted: English (US)
- Formatted: English (US)

226 This method is preferred due to its ease of use and to its high quality of interpolation. The IDW
227 interpolation is defined by:

$$228 \quad \hat{v}(x, y) = \frac{\sum_{i=1}^n w_i v_i}{\sum_{i=1}^n w_i} \quad \text{Eq. 1}$$

229 where $\hat{v}(x, y)$ is the interpolated value at point (x, y) , w_1, \dots, w_i are the relative weights and
230 v_1, \dots, v_n are the observation values. The weights are defined by the inverse distance functions:

$$231 \quad w_i = \left(\frac{r_w - d_i}{r_w d_i} \right)^2 \quad \text{Eq. 2}$$

$$232 \quad \text{for } (r_w - d_i) = \begin{cases} r_w - d_i & \text{if } d_k < r_w, \\ 0 & \text{if } d_k \geq r_w. \end{cases}$$

233 where r_w denotes the radius of influence of the point (x_i, y_i) , d_i the Euclidean distance
234 between point (x, y) and (x_i, y_i) , and d_k is the threshold distance. We used a threshold
235 distance (d_k) of 50 km, which is similar to the size of each grid cell; different d_k values were
236 included in a sensitivity study (see section 4.3). The Euclidean distance is calculated using
237 Vincenty's formulae (Vincenty, 1975). [Finally, the gridded IASI total column ammonia was re-](#)
238 [gridding to the model resolution \(\$2.5^\circ \times 1.3^\circ\$ \) using bilinear interpolation.](#)

239 2.4 Emission flux calculation of ammonia

240 The emission fluxes of ammonia were calculated using a 1-dimensional box model that
241 assumes first-order loss terms for ammonia and has been already used previously (Van Damme
242 et al., 2018; Whitburn et al., 2016b). It takes into account the gridded column concentrations of
243 ammonia that were calculated with the IDW interpolation method and all the potential removal
244 processes of ammonia occurring in a hypothetical atmospheric box according to the following
245 equation:

$$246 \quad E_{NH_3} = M_{NH_3} / \tau \quad \text{Eq. 3}$$

247 where M_{NH_3} is the mass of ammonia in each atmospheric box (grid-cell) in molecules cm^{-2} and
248 τ is the lifetime of ammonia in the box (given in seconds).

249 Van Damme et al. (2018) assumed a constant lifetime for ammonia, admitting that this is
250 a limiting factor of their study on the basis that chemical loss and deposition are highly variable
251 processes that can change the lifetime drastically. To tackle the large variability of the lifetime
252 of ammonia, we used [monthly](#) gridded lifetime calculated from a CTM. This gives robustness
253 in the calculated emissions fluxes considering that at regions where sulfuric and nitric acids are
254 abundant, the chemical loss will be more intensive, and, thus, lifetime will be much shorter
255 affecting emissions dramatically.

Deleted: e

257 The lifetime (τ) of ammonia in each grid-box results from the three processes affecting
 258 ammonia concentrations: transport (t_{trans}) in and out of the grid-cell, chemical loss (t_{chem})
 259 and deposition (t_{depo}):

$$260 \quad \frac{1}{\tau} = \frac{1}{t_{trans}} + \frac{1}{t_{chem}} + \frac{1}{t_{depo}} \quad \text{Eq. 4}$$

261 In a CTM, the lifetime can be easily calculated from the species mass balance equation (Croft
 262 et al., 2014):

$$263 \quad \frac{dC(t)}{dt} = S(t) - \frac{C(t)}{\tau(t)} \quad \text{Eq. 5}$$

264 where $C(t)$ is the atmospheric burden of ammonia at time t , $S(t)$ is the time-dependent source
 265 emission fluxes and $\tau(t)$ is the removal timescale. Assuming steady-state conditions and
 266 considering that emission fluxes of ammonia are continuous, there is a quasi-equilibrium
 267 between sources and removals of ammonia (Dentener and Crutzen, 1994), and the modeled
 268 lifetime of ammonia τ_{mod} can be defined as:

$$269 \quad \tau_{mod} = C_{NH_3} / L_{NH_3}^{trans,chem,depo} \quad \text{Eq. 6}$$

270 where C_{NH_3} is the atmospheric burden of ammonia and $L_{NH_3}^{trans,chem,depo}$ is the total loss due to
 271 any process affecting ammonia in the model (transport, chemical reactions, deposition).

272 We calculate ammonia emission fluxes using IASI satellite measurements that we
 273 interpolated (see section 2.3) to the model resolution ($2.5^\circ \times 1.3^\circ$) and applying a variable
 274 lifetime taken from a CTM (hereafter NE emissions). We also calculate ammonia emissions
 275 from the oversampled IASI data of Van Damme et al. (2018), after bilinear re-gridding to the
 276 model resolution ($2.5^\circ \times 1.3^\circ$), applying a constant lifetime for ammonia of 12 hours (hereafter
 277 VD0.5 emissions) and the same variable lifetime from a CTM as in the NE emissions (hereafter
 278 VDgrlf emissions).

279 3 Results

280 In this section, the main results of the monthly emissions (NE) are presented for the 10-
 281 year period (2008–2017) of IASI observations. We first describe the monthly modelled
 282 ammonia lifetimes (section 3.1). Then, we explain the main characteristics of the obtained
 283 emissions (section 3.2) and compare them with those calculated using the IASI gridded
 284 products from Van Damme et al. (2018) (VD0.5 and VDgrlf), as well as the ones from the state-
 285 of-the-art inventories of EGG and EDGARv4.3.1-GFED4 (Crippa et al., 2016; Giglio et al.,

Deleted: 2.2

Deleted: a

Moved up [1]: <#>LMDz-OR-INCA chemistry transport model!

The Eulerian global CTM LMDz-OR-INCA was used to calculate ammonia lifetime, as well as to simulate ammonia concentrations from the emission fluxes calculated from IASI satellite products. The model couples the LMDz (Laboratoire de Météorologie Dynamique) General Circulation Model (GCM) (Hourdin et al., 2006) with the INCA (INteraction with Chemistry and Aerosols) model (Folberth et al., 2006; Hauglustaine et al., 2004) and with the land surface dynamical vegetation model ORCHIDEE (ORGanizing Carbon and Hydrology In Dynamic Ecosystems) (Krinner et al., 2005). In the present configuration, the model has a horizontal resolution of $2.5^\circ \times 1.3^\circ$, the vertical dimension is divided into 39 hybrid vertical levels extending to the stratosphere. Large-scale advection of tracers is calculated from a monotonic finite-volume second-order scheme (Hourdin and Armengaud, 1999), deep convection is parameterized according to the scheme of Emanuel, (1991), while turbulent mixing in the planetary boundary layer (PBL) is based on a local second-order closure formalism. More information and a detailed evaluation of the GCM can be found in Hourdin et al. (2006).

The model simulates atmospheric transport of natural and anthropogenic aerosols recording both the number and the mass of aerosols. The aerosol size distribution is represented using a modal approach that consists of the superposition of 5 log-normal modes that represent both the size spectrum and whether the aerosol is soluble or insoluble (Schulz, 2007). The aerosols are treated in three particle modes, sub-micronic (diameter $< 1 \mu\text{m}$) corresponding to the accumulation mode, micronic (diameter $1-10 \mu\text{m}$) corresponding to coarse particles, and super-micronic or super coarse particles (diameter $> 10 \mu\text{m}$). LMDz-OR-INCA accounts for emissions, transport (resolved and sub-grid scale), and dry and wet (in-cloud/below-cloud scavenging) deposition of chemical species and aerosols interactively. LMDz-OR-INCA includes a full chemical scheme for the ammonia cycle and nitrate particle formation, as well as a state-of-the-art $\text{CH}_4/\text{NO}_x/\text{CO}/\text{NMHC}/\text{O}_3$ tropospheric photochemistry. Further details about specific reactions, reaction rates and other information entering into the description of the ammonia cycle can be found in Hauglustaine et al. (2014). The global transport of ammonia was simulated from 2007 to 2017 (2007 was the spin-up period) by nudging the winds of the 6-hourly ERA Interim Reanalysis data (Dee et al., 2011) with a relaxation time of 10 days (Hourdin et al., 2006). For the calculation of ammonia's lifetime, the model ran with traditional emissions for anthropogenic, biomass burning and oceanic emission sources using emissions from ECLIPSEv5-GFED4-GEIA (hereafter called EGG) (Bouwman et al., 1997; Giglio et al., 2013; Klimont et al., 2017).

Deleted: simulated

344 2013) that are often used in CTMs (section 3.3). We finally turn our focus to ~~emissions at~~
345 ~~continental~~ regions and document their seasonal variation in emissions (section 3.4).

Deleted: hot-spot

346 3.1 Modelled lifetime of ammonia

347 The lifetime of ammonia has been reported to range from a few hours to a few days
348 (Behera et al., 2013; Pinder et al., 2008) so ammonia can only be transported over relatively
349 short distances. This short spread of ammonia is also due to the fact that (a) the majority of its
350 emissions are surface ones (major source is agricultural activity), and (b) its surface deposition
351 velocities are high for most surfaces (Hov et al., 1994). The atmospheric lifetimes of ammonia
352 were summarized in Van Damme et al. (2018). Specifically, Quinn et al. (1990) and more
353 recently Norman and Leck (2005) reported lifetimes of a few hours in the West Pacific, South
354 Atlantic and Indian Oceans, which is in agreement with Flechard and Fowler (1998), who
355 reported a 2-hour lifetime in an area of Scotland where most sources are of agricultural origin.
356 Similar to them, Dammers et al. (2019) recently reported a lifetime estimated from satellite
357 measurements of 2.35 ± 1.16 hours for large point sources based on satellite measurements. The
358 majority of ammonia lifetimes reported regionally or globally fall within 10 and 24 hours
359 independently of the different approaches (Hauglustaine et al., 2014; Hertel et al., 2012; Möller
360 and Schieferdecker, 1985; Sutton et al., 1993; Whitburn et al., 2016b), while Dentener and
361 Crutzen (1994) reported slightly higher lifetimes within a range between 0.9 and 2.1 days
362 depending on ammonia emission fraction of natural origin. Monthly averaged atmospheric
363 ammonia lifetimes in the present study were derived using the version of the LMDz-OR-INCA
364 that includes non-methane hydrocarbons (Hauglustaine et al., 2004).

365 Ammonia lifetime depends on numerous factors such as the presence of ammonia's
366 reactants (~~sulfuric and nitric acids, through SO₂ and NO_x emissions~~), meteorological parameters
367 (atmospheric water vapour, and temperature, atmospheric mixing and advection) and ammonia
368 emissions. In ammonia-poor conditions, all ammonia is rapidly removed by neutralising
369 sulfuric acid with an intermediate production of bisulfate. If ammonia increases further
370 (ammonia-rich conditions), then reaction with nitric acid occurs forming nitric ammonium. At
371 this point, the ammonia/sulfuric acid/nitric acid equilibrium becomes very fragile. If sulfate
372 concentrations decrease, then free ammonia is produced, which gradually reacts with nitric acid
373 resulting in production of aerosol phase nitric ammonium. But if particles are aqueous, then
374 sulfate ions in solution increase the equilibrium vapour pressure of ammonia with nitric acid
375 reversing the reaction towards gaseous phase reactants. So, sulfate reductions are linked with

Formatted: Subscript

Deleted: sulfuric and nitric acid

Formatted: Subscript

378 non-linear increases of aerosol nitrates and decreases of aerosol ammonium and water (Seinfeld
379 and Pandis, 2000).

380 The calculated ammonia lifetime is shown in [Figure 1a averaged for the whole study](#)
381 [period](#). The average lifetime was calculated to be 11.6 ± 0.6 hours, which is in the range of the
382 previously reported values. Lower values (~ 10 hours) were observed in clean remote areas
383 characterized by low ammonia emissions (e.g., Amazon forest, Sahara and Australia), while in
384 the rest of the globe the lifetime was closer to the average value. The highest lifetimes (~ 16
385 hours) occur over Southern Brazil and Venezuela, which are both areas with relatively high
386 ammonia emissions and low sulfuric and nitric acid concentrations ([Figure 1c](#)). These
387 conditions are characterized by a low atmospheric sulfuric and nitric acids availability to
388 remove ammonia rapidly, hence causing an increase in lifetime.

389 3.2 Satellite-constrained emissions

390 The average ammonia emissions calculated from the 10-year IASI observations are
391 shown in [Figure 1b](#) (also in [Figure S 1a](#)), the reactants' atmospheric burden in [Figure 1c](#) and
392 their seasonal variability in [Figure 1d together with monthly modelled lifetimes](#). The year-by-
393 year total ammonia emissions are depicted in [Figure S 1](#), with a monthly temporal resolution.
394 Emissions decline from 242 Tg yr^{-1} in 2008 to 212 Tg yr^{-1} in 2011. In 2012 – 2014, emissions
395 show little variation (194 , 204 and 195 Tg yr^{-1} , respectively), before they increase steeply to
396 248 Tg yr^{-1} in 2015. Finally, in 2016 and 2017 they remain at the same high level (197 and 227
397 Tg yr^{-1} , respectively).

398 The global average annual emission calculated from VD0.5 amounts to 189 Tg (9-year
399 average), which is comparable to the average of the 10-year period that we have calculated in
400 the present study (average \pm sd: $213 \pm 18.1 \text{ Tg yr}^{-1}$). The increase in the emissions we calculate
401 during 2015 and 2017 stand out. The explanation for these increases could be twofold. If sulfur
402 dioxide ([a precursor of sulfates](#)) emissions decreased over time, less sulfates are available to
403 neutralize ammonia, hence resulting in higher ammonia column concentrations seen by IASI
404 that could be attributed to new emissions erroneously (see section 2.4). [This has been already](#)
405 [reported for the North China Plain To improve air quality, the Chinese government](#)
406 [implemented new emission regulations aimed at decreasing the national total NOx emissions](#)
407 [by 10% between 2011 and 2015](#) (Liu et al., 2017). [Several recent studies](#) (Duncan et al., 2016;
408 Krotkov et al., 2016) [have highlighted the effectiveness of the air quality policy, as evidenced](#)

Deleted: Figure 1

Deleted: Figure 1

Deleted: Figure 1

Deleted: Figure S 1

Deleted: Figure 1

Deleted: Figure 1

Deleted: Figure S 1

Deleted: 2.3

417 by a decreasing trend in nitrogen dioxide columns over China since 2012. The same has been
418 reported for the sulfur dioxide emissions (Elissavet Koukouli et al., 2018; Krotkov et al., 2016;
419 Wang et al., 2013). If sulfur dioxide and sulfates presented a constant year-by-year pattern or
420 even increased, then the calculated ammonia emissions would be likely realistic.

Formatted: English (US)

Field Code Changed

Formatted: Norwegian Bokmål

Formatted: Norwegian Bokmål

421 To sort out between these two possibilities, we used sulfur dioxide measurements from
422 NASA's Ozone Monitoring Instrument (OMI, Yang et al., 2007) instrument, whereas sulfate
423 column concentrations were taken from the Modern-Era Retrospective Analysis for Research
424 and Applications, Version 2 (MERRA2, Gelaro et al., 2017) reanalysis data from NASA's
425 Global Modeling and Assimilation Office (GMAO). Figure S 2 shows timeseries of column
426 concentrations of sulfur dioxide and sulfates from OMI and MERRA2 averaged globally, for
427 continental regions (Europe, North America, South America, Africa), as well as for regions
428 where ammonia emissions are particularly high (India and Southeastern Asia, North China
429 Plain). Although column concentrations of both sulfur dioxide and sulfates present strong
430 interannual variability (Figure S 2), their global concentrations show a strong decreasing trend
431 after 2015. This indicates that sulfate amounts that neutralize ammonia and form ammonium
432 sulfate, thus it is likely that the higher ammonia concentrations seen from IASI after 2015 are
433 not necessarily a result of emission increases. This is not seen from the respective precursor of
434 the atmospheric nitric acid, nitrogen dioxide (Figure S 2).

Deleted: Figure S 2

Deleted: y do not show significant changes on an annual basis...

Deleted: are rather constant from year to year and

Deleted: retrieved

Deleted: the

Deleted: an

435 Looking closely into regions with large changes in ammonias reactants and/or their
436 precursors after 2015 (Figure 2), we immediately see that a region of interest is the North China
437 Plain. The North China Plain has been identified as an ammonia hotspot mainly due to extensive
438 agricultural activities (Clarisse et al., 2009; Pan et al., 2018). Liu et al. (2018) reported a sulfur
439 dioxide reduction of about 60% over the recent few years in the North China Plain, sulfates
440 decreased by 50%, while ammonia emissions declined by only 7% due to change in agricultural
441 practices. The suggested decrease in ammonia reactants over the North China Plain is illustrated
442 by the calculated sulfur dioxide column concentration anomaly from OMI (Figure 2) and by
443 the sulfate concentration anomaly from MERRA-2 after 2015 (the highest calculated one)
444 (Figure S 3). Nitrogen dioxide concentration do not show any noticeable annual change, despite
445 their strong seasonal cycle (Figure S 2). The IASI-constrained ammonia emissions calculated
446 here show only a tiny increase of 0.19 ± 0.04 kt y^{-1} after 2015 in the North China Plain and of
447 10 ± 3.1 Tg y^{-1} globally with respect to the 10-year average (Figure 2). This is due to the change
448 of sulfur dioxide and nitrogen oxide emission regulations in China, which in turn led to reduced

Deleted: Another

Deleted: , as

Deleted: it

Deleted: Figure 2

Deleted: Figure S 3

Deleted: However, t

Deleted: Figure 2

Deleted: SO2

Deleted: NOx

465 inorganic matter (sulfates, nitrates and ammonium) resulting in regional increases of gaseous
466 ammonia (Lachatre et al., 2019).

467 3.3 Comparison with traditional emission datasets

468 In this section, we quantify the main differences of our IASI-constrained emission dataset
469 with other state-of-the-art inventories used in global models and for different applications (air
470 quality, climate change etc...). Aside from comparing our emissions with those calculated using
471 Van Damme et al. (2018) data with a constant lifetime (hereafter called VD0.5), we extend our
472 comparison to more traditional datasets such as those of ECLIPSEv5-GFED4-GEIA (EGG) for
473 2008–2017, and EDGARv4.3.1-GFED4 (Crippa et al., 2016; Giglio et al., 2013) for 2008–2012
474 period. Finally, the ammonia emissions presented in this study (NE emissions) are compared
475 to emissions calculated from Van Damme et al. (2018) gridded IASI column data applying a
476 variable (modelled) ammonia lifetime presented in [Figure 1b](#) (hereafter referred as VDgrlf).

477 The 10-year comparison of our calculated emissions with VD0.5 is shown in [Figure 3](#).
478 The 10-year average difference amounts to $29 \pm 15 \text{ Tg yr}^{-1}$ (average \pm sd). In all years, the largest
479 differences could be seen over Latin America and over tropical Africa. Our emissions (NE)
480 [show a different structure](#) in the Indo-Gangetic Plain, and situated slightly more northerly [than](#)
481 [those in VD0.5](#). [The difference might be due to the IDW interpolation used to process the IASI](#)
482 [ammonia in the NE emissions compared with the oversampling method used in VD0.5 \(see](#)
483 [section 2.3\)](#). Nevertheless, Northern India has been identified as a hot-spot region for ammonia,
484 mainly due the importance of agricultural activities in the region (Kuttippurath et al., 2020;
485 Tanvir et al., 2019).

486 [Figure S 4](#) and [Figure S 5](#) present a comparison of our calculated emissions (NE) with
487 the basic state-of-the-art datasets of EGG and EDGARv4.3.1-GFED4, respectively. In both
488 datasets, ammonia emissions remain almost constant over time (average \pm sd: $65 \pm 2.8 \text{ Tg yr}^{-1}$
489 and $103 \pm 5.5 \text{ Tg yr}^{-1}$, respectively). The total calculated ammonia emissions [in EGG and](#)
490 [EDGARv4.3.1-GFED4](#) are up to three times lower than those calculated from NE (average \pm sd:
491 $213 \pm 18.1 \text{ Tg yr}^{-1}$) or from VD0.5 (9-year average: 189 Tg yr^{-1}). This results in 10-year annual
492 differences that are very significant (average \pm sd: $150 \pm 19.3 \text{ Tg yr}^{-1}$ and $111 \pm 19.2 \text{ Tg yr}^{-1}$,
493 respectively); the largest differences appear over South America ([EGG: \$7.1 \pm 0.3 \text{ Tg yr}^{-1}\$, VD0.5:](#)
494 [\$22 \text{ Tg yr}^{-1}\$, NE: \$28 \pm 3.0 \text{ Tg yr}^{-1}\$, VDgrlf: \$24 \pm 1.3 \text{ Tg yr}^{-1}\$](#)), while European emissions are
495 practically identical in all datasets [except EGG \(EGG: \$6.9 \pm 1.1 \text{ Tg yr}^{-1}\$, VD0.5: \$11 \text{ Tg yr}^{-1}\$, NE:](#)

Deleted: Figure 1

Deleted: Figure 3

Deleted: were lower

Deleted: ,

Deleted: previously

Deleted: Figure S 4

Deleted: Figure S 5

503 $15\pm 2.2 \text{ Tg yr}^{-1}$, $\text{VDgrlf: } 11\pm 1.0 \text{ Tg yr}^{-1}$). Emissions from South China Plain are much higher in
504 the two traditional datasets that those presented in this paper (EGG: $25\pm 1.2 \text{ Tg yr}^{-1}$, $\text{VD0.5: } 36$
505 Tg yr^{-1} , $\text{NE: } 38\pm 2.8 \text{ Tg yr}^{-1}$, $\text{VDgrlf: } 39\pm 1.8 \text{ Tg yr}^{-1}$). Ammonia emissions derived over China
506 in this work (NE) are among the highest worldwide (Figure S 1), which agrees well with the 9-
507 year average emissions calculated in VD0.5 inventory over China (see Figure 3). To assess to
508 which extent emissions from EGG and EDGARv4.3.1-GFED4 are underestimated can only be
509 done by comparing ammonia with ground or satellite observations.

510 The comparison of the annual ammonia emissions in the NE dataset to the modified
511 VDgrlf emissions is shown in Figure S 6. The latter showed a better agreement to the emissions
512 presented in this study with mean annual different of $14\pm 19 \text{ Tg yr}^{-1}$ (average \pm sd). Previously
513 observed emission differences in the two state-of-the-art inventories over South America and
514 Africa have been now minimized, as well as the displacement north of the Indo-Gangetic Plain
515 emissions remains important. Nevertheless, the smaller differences of our emissions (NE) from
516 those of VDgrlf as compared with the respective difference from the VD0.5 emissions, show
517 the large impact that a more realistic variable lifetime might have in emission calculations with
518 this methodology in these regions.

519 3.4 Site-specific ammonia emissions and seasonal variation

520 Figure 4 illustrates specific regions that show the largest ammonia emissions (Europe,
521 North America, South America and Southeastern Asia). These emissions correspond to the
522 IASI-constrained emissions calculated in this study (NE) and are presented as total annual
523 emissions averaged over the 10-year period of study. At the bottom panels of the same figure,
524 the seasonal variation of the emissions is shown for each of the four hot-spot regions and each
525 of the 10 years of the study.

526 European total ammonia emissions were estimated to be $15\pm 2.2 \text{ Tg yr}^{-1}$ (average \pm sd),
527 more than double compared with those reported in EGG ($6.9\pm 1.1 \text{ Tg yr}^{-1}$) and similar to those
528 in VD0.5 (11 Tg yr^{-1}) or those in VDgrlf ($11\pm 1.0 \text{ Tg yr}^{-1}$). The greatest emissions were
529 calculated for Belgium, the Netherlands and the Po Valley in Italy (Figure 4). High emissions
530 are also found in North and Northwestern Germany and over Denmark. In contrast, very low
531 emissions are found in Norway, Sweden and parts of the Alps. It is not possible to quantitatively
532 distinguish between different sources of ammonia. It has been reported that approximately 75%
533 of ammonia emissions in Europe originate from livestock production (Webb et al., 2005), and

Deleted: calculated here

Deleted: Based upon IASI retrievals, Liu et al. (2019) showed an increase of surface NH_3 concentrations trend of more than $0.2 \mu\text{g N m}^{-3} \text{ yr}^{-1}$ in eastern China and of around $0.1\text{--}0.2 \mu\text{g N m}^{-3} \text{ yr}^{-1}$ in northern Xinjiang during 2008–2016.

Deleted: Figure S 1

Deleted: Figure 3

Deleted: Figure S 6

Deleted:

Deleted: Figure 4

Formatted: Font: Bold

Deleted: Figure 4

545 90% from agriculture in general (Leip et al., 2015). More specifically, ammonia is emitted from
546 all stages of manure management, from livestock buildings during manure storage and
547 application to land, as well as from livestock urine. These emissions are strong over most of
548 Northwestern European countries, although sources like fertilization and non-agricultural
549 activities (traffic and urban emissions) can be also important. An example is Tange in Germany,
550 which shows a late summer peak due to growing crops application. No obvious seasonality in
551 the emissions can be seen for Europe as a whole, as the hot-spot regions are rather few compared
552 to the overall surface of Europe. An exception to this stable emission situation over the year
553 occurs during 2010 and during 2015, years for which a late summer peak. In 2010, large
554 wildfires in Russia resulted in high ammonia emissions (R'Honi et al., 2013), while year 2015
555 has been also characterized as an intense fire year (though not like 2010), with fires occurring
556 in Eurasia (Min Hao et al., 2016).

557 North America and in particular the US (Figure 4) has been characterized by four hot-
558 spot regions. First, a small region in Colorado, Central US, which is the location of a large
559 agricultural region that traditionally releases large ammonia emissions (Malm et al., 2013).
560 Another example is the state of Iowa (home to more than 20 million swine, 54 million chickens,
561 and 4 million cattle), northern Texas and Kansas (beef cattle), and southern Idaho (dairy cattle)
562 (McQuilling, 2016). Furthermore, the three major valleys in Salt Lake, in Cache, and in Utah
563 in the midwestern US show an evident, but lower intensity hot-spot, as they are occupied by
564 massive pig farms associated to open waste pits. The largest emissions were calculated for the
565 San Joaquin Valley in California (vegetables, dairy, beef cattle and chickens) and further to the
566 South (Tulare and Bakersfield), an area characterized by feedlots (Van Damme et al., 2018;
567 McQuilling, 2016). North American annual ammonia emissions over the 10-year period were
568 averaged $1.1 \pm 0.1 \text{ Tg yr}^{-1}$ (average \pm sd). These values are over two orders of magnitude higher
569 than those in EGG ($0.062 \pm 0.0013 \text{ Tg yr}^{-1}$). Note that his estimate is three times lower than those
570 reported in VD0.5 (3.1 Tg yr^{-1}) or in VDgrlf ($3.4 \pm 0.5 \text{ Tg yr}^{-1}$). The 2008–2017 interannual
571 variability (Figure 4) all show a minimum in winter. Maximum emissions were observed in late
572 spring, due to the contribution from mineral fertilizer and manure application, in summer, due
573 to influence of livestock housing emissions, and some years both in spring and summer (Makar
574 et al., 2009; Zhu et al., 2013, 2015). A topographical dependence was also seen in midwest
575 emissions that peaked in April, whereas over the rest of the US maximum emissions were
576 appeared in summer (Paulot et al., 2014).

Deleted: Figure 4

Deleted: Figure 4

579 Ammonia emissions have different characteristics in South America and in Western
580 Africa as both are fire-dominated regions. For simplicity we only present South America in
581 **Figure 4**. This region is dominated by natural ammonia emissions mainly from forest, savanna
582 and agricultural fires (Whitburn et al., 2014, 2016b) and volcanoes (Kajino et al., 2004;
583 Uematsu et al., 2004). This causes a strong seasonal variability in the ammonia emissions with
584 the largest fluxes observed from August to October in all years (**Figure 4**). This strong
585 dependence of South America from biomass burning emissions was first highlighted by Chen
586 et al. (2013) and by van Marle et al. (2017). It also became particularly pronounced during the
587 large wildfires in the Amazon rainforest in summer 2019 (Escobar, 2019). We estimated the
588 10-year average ammonia emissions to be $28 \pm 3.0 \text{ Tg yr}^{-1}$ (average \pm sd) in agreement with
589 VD0.5 (22 Tg yr^{-1}) and VDgrlf ($24 \pm 1.3 \text{ Tg yr}^{-1}$). The respective emissions in EGG are four
590 times lower than these estimates ($7.1 \pm 0.3 \text{ Tg yr}^{-1}$).

Deleted: Figure 4

Deleted: Figure 4

591 The last column to the right of **Figure 4** presents the 10-year average annual ammonia
592 emissions and their respective interannual variability in Southeastern Asia. We define this
593 region spanning from 70°E – 130°E in longitude and from 0°N – 45°N in latitude. Ammonia
594 emissions were estimated to be $38 \pm 2.8 \text{ Tg yr}^{-1}$ (average \pm sd) similar to VD0.5 (36 Tg yr^{-1}) and
595 VDgrlf ($39 \pm 1.8 \text{ Tg yr}^{-1}$) and slightly higher than those presented in EGG ($25 \pm 1.2 \text{ Tg yr}^{-1}$). They
596 comprise ammonia fertilizer plants, such as in Pingsongxiang, Shizuishan, Zezhou-Gaoping,
597 Chaerhan Salt Lake, Delingha, Midong-Fukang and Wucaiwan (China), Indo-Gangetic Plain
598 (Pakistan and India), Gresik (Indonesia). China and India contribute more than half of total
599 global ammonia emissions since the 1980s with the majority of these emissions to originate
600 from rice cultivation followed by corn and wheat (crop-specific emissions). More specifically,
601 emissions from these crops due to synthetic fertilizer and livestock manure applications are
602 concentrated in North China Plain (Xu et al., 2018). Considering that Southeastern Asia is the
603 largest agricultural contributor in the global ammonia budget, a strong seasonality in the
604 emissions was observed. Temporal ammonia emissions peak in late summer of most years,
605 when emissions from rice cultivation, synthetic fertilizer application and livestock manure
606 spreading (Xu et al., 2016) are important, and in spring when wheat cultivation dominates
607 (Datta et al., 2012). Of course, the respective emissions from biomass burning should also be
608 mentioned. However, these are difficult to be distinguish and are expected to be a relatively
609 small source compared to agricultural emissions.

Deleted: Figure 4

613 4 Discussion

614 In this section, we conduct simulations over the 10-year period (2008–2017, 1-year spin-
615 up), with all the emissions derived and compare the NH₃ concentrations with ground-based
616 observations over Europe, North America, Southeastern Asia (section 4.1), and observations
617 from CrIS (section 4.2). These simulations consist in: (i) a simulation using traditional
618 emissions using EGG; (ii) a simulation using emissions calculated from IASI data from Van
619 Damme et al. (2018) applying a constant lifetime of 12 hours for ammonia (VD0.5); (iii) a
620 simulation using gridded emissions presented in the present paper (NE) calculated as described
621 in section 2; and (iv) a simulation using emissions calculated from IASI data from Van Damme
622 et al. (2018) applying a variable (modelled) lifetime (VDgrlf). Finally, we perform a sensitivity
623 analysis in order to define the levels of uncertainty of our emissions in section 4.3 and discuss
624 potential limitation of the present study in section 4.4.

625 4.1 Validation against ground-based observations

626 **Figure 5** shows a comparison between modelled surface concentrations of ammonia with
627 ground measurements from Europe (EMEP, <https://emep.int/mscw/>), North America (AMoN,
628 <http://nadp.slh.wisc.edu/data/AMoN/>) and Southeastern Asia (EANET,
629 <https://www.eanet.asia>). To avoid overplotting, the Gaussian kernel density estimation (KDE)
630 was used, which is a non-parametric way to estimate the probability density function (PDF) of
631 a random variable (Parzen, 1962):

$$632 \quad f(x) = \frac{1}{Nh} \sum_{i=1}^N K\left(\frac{x-x_i}{h}\right) \quad \text{Eq. 7}$$

633 where K is the kernel, x_i the univariate independent and identically distributed point of the
634 relationship between modelled and measured ammonia and h is a smoothing parameter called
635 the bandwidth. KDE is a fundamental data smoothing tool that attempts to infer characteristics
636 of a population, based on a finite dataset. It weighs the distance of all points in each specific
637 location along the distribution. If there are more points grouped locally, the estimation is higher
638 as the probability of seeing a point at that location increases. The kernel function is the specific
639 mechanism used to weigh the points across the data set and it uses the bandwidth to limit the
640 scope of the function. The latter is computed using the Scott's factor (Scott, 2015). We also
641 provide the mean fractional bias (MFB) for modelled and measured concentrations of ammonia
642 as follows:

$$643 \quad MFB = \frac{1}{N} \frac{\sum_{i=1}^N (C_m - C_o)}{\sum_{i=1}^N \left(\frac{C_m + C_o}{2}\right)} \times 100\% \quad \text{Eq. 8}$$

Deleted: ground based

Deleted: of

Deleted: from

Deleted: ECLIPSEv5 (Evaluating the CLimate and Air Quality ImPacts of Short-livEd Pollutants) for anthropogenic sources, GFED4 (Global Fire Emission Dataset) for biomass burning emissions and GEIA (Global Emissions Initiative) for oceanic sources from (Bouwman et al., 1997; Giglio et al., 2013; Klimont et al., 2017), where modelled lifetimes of ammonia were also calculated (...)

Deleted:)

Formatted: Font: Bold

Deleted: Figure 5

656 where C_m and C_o are the modelled and measured ammonia concentrations and N is the total
 657 number of observations. MFB is a symmetric performance indicator that gives equal weights
 658 to under- or over-estimated concentrations (minimum to maximum values range from -200%
 659 to 200%). Furthermore, we assess the deviation of the data from the line of best fit using the
 660 root mean square error (RMSE) defined as:

$$661 \quad RMSE = \sqrt{\sum_{i=1}^N \frac{(C_m - C_o)^2}{N}} \quad \text{Eq. 9}$$

662 From 134 European stations, nearly 300,000 measurements made at a daily to weekly
 663 temporal resolution over the period of study (2007–2018) are presented on **Figure 5**. All
 664 emission datasets underestimate ammonia surface concentration over Europe. The most
 665 accurate prediction of concentrations was achieved using the traditional EGG emissions that
 666 underestimated observations by 67%, also being the least scattered from the best fit
 667 ($RMSE_{EGG} = 4.06 \mu\text{g N m}^{-3}$), followed by the emissions presented in this paper ($MFB_{NE} =$
 668 -72% , $RMSE_{NE} = 4.65 \mu\text{g N m}^{-3}$), although they were more variable. VD0.5 or VDgrlf
 669 emissions further underestimated observations, though they were less sparse (**Figure 5d**). About
 670 12% of the modelled concentrations using EGG were outside of the 10-fold limit from the
 671 observations, in contrast to only 17% and 15% in VD0.5 and VDgrlf, and 20% in NE. With
 672 regards to the spatial comparison with the observed concentrations, all datasets cause
 673 overestimations in the ammonia concentrations predicted in Eastern Europe (station
 674 AM0001R). EGG appears to be the most accurate in Central Europe (all stations with suffix
 675 DE00), NE emissions in all Spanish stations (suffix ES00) and VD0.5 and VDgrlf emissions in
 676 Italian stations (**Figure S 7**).

677 The comparison of simulated ammonia concentrations to observations over North
 678 America includes 119 stations, which represent nearly 27,000 observations (**Figure 6**) with a
 679 weekly, bi-weekly or monthly resolution. The only emission dataset that lead to an
 680 underestimation of ammonia concentrations was EGG ($MFB_{EGG} = -28\%$). Two others,
 681 VD0.5 and VDgrlf caused ammonia observations to be strongly overestimated ($MFB_{VD0.5} =$
 682 **52% and $MFB_{VDgrlf} = 54\%$**), while NE slightly ($MFB_{NE} = 32\%$). All inventories resulted
 683 in about the same variability in ammonia concentrations with RMSEs between 4.15 and 4.17
 684 $\mu\text{g N m}^{-3}$ (**Figure 6**). About 10% of the predicted concentrations using EGG emissions were at
 685 least 10 times off from the measured ones, more than twice the number of measurements
 686 compared to the other dataset. NE emissions better capture levels in the easternmost stations of
 687 the US (AL99, AR15, CT15, IL37, IN22, MI52, NY56, ON26) and in California (CA83) and

Formatted: Font: Bold

Deleted: Figure 5

Deleted: Figure 5

Formatted: Font: Bold

Deleted: Figure S 7

Formatted: Font colour: Black, Shadow

Deleted: Figure 6

Formatted: Font: Font colour: Black, Text Outline, Shadow

Deleted: Figure 6

693 Oklahoma (OK98), which are close to hot-spot regions (see section 3.4). EGG emissions
694 perform better in Northwestern (ID03), Central (KS03) and several stations located over the
695 Eastern United States (KY03, KY98, OH09, AR03, IL46, KS03, GA41). The emission
696 inventory VD0.5 leads to a very good agreement in ammonia concentrations over all stations
697 of the North American continent (AL99, GA40, ID03, GA41, IL37, IL46, IN20, IN22, KS97,
698 PA00, MD99, MI52, TN04, NM99, NY96, OH99, OK98) (Figure S 8).

Deleted: Figure S 8

Formatted: Font: Font colour: Black, Text Outline, Shadow

699 In Southeastern Asia 62 stations from 13 countries were included in the comparison from
700 the EANET monitoring network (Figure 7). These included about 8,000 surface measurements
701 in monthly or 2-weekly resolution. All emission inventories underestimate station
702 concentrations of EANET with MFBs between -102% (EGG) and -61% (VD0.5 and VDgrlf).
703 The least spread model concentrations were those simulated using VD0.5 and VDgrlf
704 ($RMSE = 4.61 - 4.65 \mu g N m^{-3}$). Around 19% of model concentrations using EGG were
705 outside the 10-fold limit of the 1×1 line with observations, 12% using NE emissions and only
706 5% and 6% using VD0.5 and VDgrlf, respectively. VD0.5 and VDgrlf emissions capture well
707 the Japanese (suffix JPA) and Taiwanese stations (suffix THA). Given the short lifetime and
708 the relatively coarse spatial scales, the model fails to capture the variability that exists within
709 each gridbox (Figure S 9).

Deleted: Figure 7

Deleted: ()

Formatted: Font: 12 pt, Not Bold, Font colour: Black, Text Outline, Shadow

Deleted: Figure S 9

710 4.2 Validation against satellite products

711 Here, we used surface ammonia concentrations from CrIS from 1st May 2012 to 31st
712 December 2017 and we compared them with modelled ammonia concentrations using four
713 emissions datasets (EGG, VD0.5, NE and VDgrlf), like in the previous section **but in global**
714 **scale**. The comparison is shown as PDF of surface modelled against CrIS concentrations of
715 ammonia calculated with the Gaussian KDE in Figure 8. A total of 4.5 million surface
716 measurements were used in the comparison with a global coverage. All datasets underestimated
717 surface concentrations except NE emissions, which overestimate ammonia ($MFB = +0.48$).
718 The best fit was achieved for the VDgrlf emissions, which slightly underestimate ammonia
719 ($MFB = -0.37$), while 82% of the measurements were within one order of magnitude from
720 the 1×1 line, which is also shown by the small $RMSE$. VD0.5 emissions produced similar
721 concentrations, with respect to the $RMSE$ and MFB values, whereas 79% of them were less
722 than a 10-fold difference from the observations. NE emissions result in higher surface
723 concentrations, also showing larger $RMSEs$. However, 90% of the modelled concentrations
724 were within a factor of 10 from the CrIS observation. In general, a better agreement for the

Deleted: Figure 8

730 most recent years 2015 – 2017 was achieved. The baseline EGG emissions resulted in
731 significantly larger deviations of modelled surface concentrations of ammonia from the CrIS
732 observations, as shown in **Figure 8**, comprising the largest *RMSE* and *MFB* values.

Deleted: Figure 8

733 4.3 Uncertainty analysis

734 A sensitivity analysis in order to calculate the level of uncertainty that each of the
735 parameter gives to the modelled surface concentrations of ammonia was also performed. The
736 relative uncertainty was calculated as the standard deviation of ammonia's surface
737 concentrations from a model ensemble of 10 members (**Table 1**) divided by the average. The
738 first six members are the surface concentrations that resulted from simulations of ammonia
739 emissions after perturbation of the Euclidian distance d_k in the parameters of the IDW
740 interpolation. The remaining four members are simulated concentrations using the previously
741 reported emissions datasets (EGG, VD0.5, NE and VDgrlf). The results are shown as a 10-year
742 (2008–2017) annual average relative uncertainty in **Figure 9**, and as annual average relative
743 uncertainty of surface concentrations for every year of the 10-year period in **Figure S 10**,

Deleted: Table 1

Deleted: Figure 9

Deleted: Figure S 10

744 The surface concentrations resulting from the different calculated emissions mainly
745 affects oceanic regions, with values reaching 100%. The reason for this could be threefold.
746 First, the IDW interpolation shows to be affected by severe outlier values, which are found in
747 several oceanic regions (**Figure S 11**); this creates high gridded column ammonia
748 concentrations and, in turn, fluxes at regions that are not supported by previous findings or
749 measurements. Second, the methodology with which ammonia concentrations are retrieved in
750 IASI has certain limitation, with respect to (i) the use of constant vertical profiles for ammonia,
751 (ii) potential dependencies of total column ammonia and temperature that are not taken into
752 account, and (iii) instrumental noise that can cause bias (Whitburn et al., 2016a). Third, there
753 is much less ammonia over the Ocean, hence the relative error bars are much larger. Large
754 uncertainties in surface ammonia concentrations were observed in regions characterized by
755 large anthropogenic contribution, such as North India, North China Plain and Central USA.
756 Smaller uncertainties were found in Central Africa and in Amazonia, regions that are linked
757 with episodic biomass burning emissions (**Figure 4**).

Deleted: Figure S 11

Deleted: a high

Deleted: of the measurements

Deleted: Figure 4

758 4.4 Limitations of the present study

759 We discuss the importance of certain limitations in the methodology of the present study
760 and in the validation of the results. These limitations will also be commented upon in the overall
761 conclusion of the paper.

770 Regarding the methodology, emissions of short-lived species are determined, among
771 other methods, using top-down approaches. When only satellite measurements are available,
772 they are usually averaged over a particular location and surface emissions are calculated using
773 a mass balance approach (Lin et al., 2010; Zhao and Wang, 2009). This is done by assuming a
774 1-dimensional box-model, where atmospheric transport between grids is assumed to be
775 negligible and loss due to deposition or chemical reactions very fast. The solution to this
776 problem is the use of Kernels (Boersma et al., 2008), which makes the computation of the
777 emissions very intense. It has been reported that for resolutions, such as those used in the
778 present paper ($2.5^{\circ} \times 1.3^{\circ}$), non-local contributions to the ammonia emissions are relatively
779 small (Turner et al., 2012). Although, the use of Kernels is the proper way to account for non-
780 local contributions, we believe that negligible transport here is a fair assumption, due to the
781 small lifetimes of ammonia calculated from the CTM (11.6 ± 0.6 hours); therefore,
782 transportation from the adjacent grid-cells should be small. Note that ~~although~~ this method has
783 been suggested for short lived climate pollutants, it is not suitable for species with lifetime from
784 days to weeks (e.g. black carbon, Bond et al., 2013).

Deleted: already

785 Another limitation of the present study is that the same model is used for the calculation
786 of the modelled lifetimes and for the validation of the emissions that were calculated using
787 these lifetimes (NE and VDgrlf). A more accurate validation would require an independent
788 model for the simulations of surface concentrations using these emissions. ~~Nevertheless, the~~
789 ~~IASI-constrained emissions of ammonia presented here are publicly available for use in global~~
790 ~~models.~~

791 5 Conclusions

792 In the present paper, satellite measurements from IASI were used to constrain global
793 ammonia emissions over the period 2008–2017. The data were firstly processed to monthly
794 ammonia column concentrations with a spatial resolution of $2.5^{\circ} \times 1.3^{\circ}$. Then, using gridded
795 lifetime for ammonia calculated with a CTM, monthly fluxes were derived. This contrasts with
796 previously reported methods that used a single constant lifetime. This enables a more accurate
797 calculation in regions ~~where different abundances of atmospheric sulfuric and nitric acid, as~~
798 ~~well as in their precursors (sulfur and nitrogen dioxide, respectively) can neutralize ammonia~~
799 ~~through heterogeneous chemical reactions to sulfate and nitrate aerosols.~~ The calculated
800 ammonia emission fluxes were then used to simulate ammonia concentrations for the period
801 2008–2017 (referred to as NE). The same simulations were repeated using baseline emissions
802 from ECLIPSEv5-GFED4-GEIA (referred to as EGG), emissions constrained by Van Damme

Deleted: sensitive to the changing balance between

Deleted: nitrate and sulfate

Deleted: abundances

807 et al. (2018) IASI data using a constant lifetime for ammonia (named as VD0.5) and emissions
808 based on Van Damme et al. (2018) retrievals using a modelled lifetime from a CTM (named as
809 VDgrlf). The simulated surface concentrations of ammonia were compared with ground
810 measurements over Europe (EMEP), North America (AMoN) and Southeastern Asia (EANET),
811 as well as with global satellite measurements from CrIS. The main conclusions can be
812 summarized as follows:

- 813 • The 10-year average annual ammonia emissions calculated here (NE) were estimated to be
814 $213 \pm 18.1 \text{ Tg yr}^{-1}$, which is 15% higher than those in VD0.5 (189 Tg yr^{-1}), and 6% higher
815 than those in VDgrlf ($201 \pm 10.4 \text{ Tg yr}^{-1}$). These emission values amount to twice the
816 published from datasets, such as EGG ($65 \pm 2.8 \text{ Tg yr}^{-1}$) and EDGARv4.3.1-GFED4,
817 ($103 \pm 5.5 \text{ Tg yr}^{-1}$).
- 818 • In the North China Plain, a region characterized by intensive agricultural activities, a small
819 increase of ammonia emissions is simulated after 2015. This is attributed to decreases in
820 sulfur species, as revealed from OMI and MERRA-2 measurements. Less sulfates in the
821 atmosphere leads to less ammonia neutralization and hence to larger loads in the
822 atmospheric column as measured by IASI.
- 823 • In Europe, the 10-year average of ammonia emissions were estimated at $15 \pm 2.2 \text{ Tg yr}^{-1}$
824 (NE), twice as much as those in EGG ($6.9 \pm 1.1 \text{ Tg yr}^{-1}$) and similar to those in VD0.5 (11
825 Tg yr^{-1}) or VDgrlf ($11 \pm 1.0 \text{ Tg yr}^{-1}$). The strongest emission fluxes were calculated over
826 Belgium, Netherlands, Italy (Po Valley), Northwestern Germany and Denmark. These
827 regions are known for industrial and agricultural applications, animal breeding activities,
828 manure/slurry storage facilities and manure/slurry application to soils.
- 829 • Some hot-spot regions with high ammonia emissions were distinguished in North America:
830 (i) in Colorado, due to large agricultural activity, (ii) in Iowa, northern Texas and Kansas,
831 due to animal breeding, (iii) in Salt Lake, Cache, and Utah, due to animal farms associated
832 with open waste pits and (iv) in California, due to animal breeding and agricultural
833 practices. Ammonia emissions in North America were $1.1 \pm 0.1 \text{ Tg yr}^{-1}$ or two orders of
834 magnitude higher than in EGG ($6.2 \pm 0.1 \text{ kt yr}^{-1}$) and three times lower than those in VD0.5
835 (3.1 Tg yr^{-1}) or in VDgrlf ($3.4 \pm 0.5 \text{ Tg yr}^{-1}$), with maxima observed in late spring, due to
836 fertilization and manure application and summer, due to livestock emissions.
- 837 • South America is dominated by natural ammonia emissions mainly from forest, savanna
838 and agricultural fires causing a strong seasonality with the largest fluxes between August
839 and October. The 10-year average ammonia emissions were as high as $28 \pm 3.0 \text{ Tg yr}^{-1}$

840 similar to VD0.5 (22 Tg yr⁻¹) and VDgrlf (24±1.3 Tg yr⁻¹) and four times higher than EGG
841 (7.1±0.3 Tg yr⁻¹).

- 842 • In Southeastern Asia, the 10-year average ammonia emissions were 38±2.8 Tg yr⁻¹, in
843 agreement with VD0.5 (36 Tg yr⁻¹) and VDgrlf (39±1.8 Tg yr⁻¹) and slightly higher than
844 those in EGG (25±1.2 Tg yr⁻¹). The main sources were from fertilizer plants in China,
845 Pakistan, India and Indonesia. China and India hold the largest share in the ammonia
846 emissions mainly due to rice, corn and wheat cultivation. A strong seasonality in the
847 emissions was observed with a late summer peak in most years, due to rice cultivation,
848 synthetic fertilizer and livestock manure applications and in spring due to wheat
849 cultivation.
- 850 • About 88% of the modelled concentrations over Europe using EGG were inside the 10-
851 fold limit from the observations, higher than those with VD0.5 (83%), VDgrlf (85%) and
852 NE (80%). All emission datasets overestimate of ammonia in Eastern Europe, EGG
853 captures better Central Europe, NE emissions predict concentrations in Spain and VD0.5
854 with VDgrlf emissions in Italy.
- 855 • In North America, 90% of the modelled concentrations using EGG emissions were less
856 than 10 times different from the measured ones; more than 95% of the modelled
857 concentrations in North American stations were in the same range using NE, VD0.5 and
858 VDgrlf emissions. NE emissions better capture levels in the easternmost stations of the US
859 closer to the respective hot-spot regions, whereas EGG emissions perform better in
860 Northwestern and Central USA. VD0.5 and VDgrlf emissions perform well in most of the
861 North American stations.
- 862 • All emissions underestimate station concentrations in Southeastern Asia. The least spread
863 model concentrations were those simulated using VD0.5 and VDgrlf. About 81% of
864 modelled concentrations using EGG were in the 10-fold limit of the 1×1 line with
865 observations, 88% using NE and only 95% and 94% using VD0.5 and VDgrlf, respectively.
866 VD0.5 and VDgrlf emissions capture well the Japanese and Taiwanese stations.
- 867 • The comparison of the modelled ammonia with satellite observations from CrIS globally
868 showed that the best agreement was achieved using the VDgrlf emissions in 2012–2014.
869 After 2015, all satellite retrieved emissions show a better agreement with CrIS
870 concentrations.

871 Overall, the satellite-constrained ammonia emissions calculated using a variable lifetime
872 appear to give more realistic concentrations, with respect to station and satellite measurements.
873 Accordingly, state-of-the-art emissions appear to underestimate ammonia significantly.

874

875 *Data availability.* All data and python scripts used for the present publication are open through
876 the web address <https://folk.nilu.no/~nikolaos/AMMONIA/> or can be obtained from the
877 corresponding author upon request.

878

879 *Competing interests.* The authors declare no competing interests.

880

881 *Acknowledgements.* This study was supported by the Research Council of Norway (project
882 ID: 275407, COMBAT – Quantification of Global Ammonia Sources constrained by a
883 Bayesian Inversion Technique). Lieven Clarisse and Martin Van Damme are respectively a
884 research associate and a postdoctoral researcher supported by the F.R.S.–FNRS.

885

886 *Author contributions.* N.E. performed the simulations, analyses, wrote and coordinated the
887 paper. S.E. contributed to the lifetime calculations. Y.B., D.H. and A.C. set up the CTM model.
888 M.V.D., P.-F.C. and L.C. provided the IASI data, while M.W.S. and K.E.C.-P. provided the
889 observations from CrIS. All authors contributed to the final version of the manuscript.

890

891 **References**

- 892 Abbatt, J. P. D., Benz, S., Cziczo, D. J., Kanji, Z., Lohmann, U. and Mohler, O.: Solid
893 Ammonium Sulfate Aerosols as Ice Nuclei: A Pathway for Cirrus Cloud Formation,
894 *Science* (80-.), (September), 1770–1773, 2006.
- 895 Anderson, N., Strader, R. and Davidson, C.: Airborne reduced nitrogen: Ammonia
896 emissions from agriculture and other sources, *Environ. Int.*, 29(2–3), 277–286,
897 doi:10.1016/S0160-4120(02)00186-1, 2003.
- 898 Aneja, V. P., Schlesinger, W. H. and Erisman, J. W.: Farming pollution, *Nat. Geosci.*,
899 1(7), 409–411 [online] Available from: <http://dx.doi.org/10.1038/ngeo236>, 2008.
- 900 Aneja, V. P., Schlesinger, W. H. and Erisman, J. W.: Effects of agriculture upon the
901 air quality and climate: Research, policy, and regulations, *Environ. Sci. Technol.*,
902 43(12), 4234–4240, doi:10.1021/es8024403, 2009.
- 903 August, T., Klaes, D., Schlüssel, P., Hultberg, T., Crapeau, M., Arriaga, A., O'Carroll,
904 A., Coppens, D., Munro, R. and Calbet, X.: IASI on Metop-A: Operational Level 2
905 retrievals after five years in orbit, *J. Quant. Spectrosc. Radiat. Transf.*, 113(11),
906 1340–1371, doi:10.1016/j.jqsrt.2012.02.028, 2012.
- 907 Behera, S. N., Sharma, M., Aneja, V. P. and Balasubramanian, R.: Ammonia in the
908 atmosphere: A review on emission sources, atmospheric chemistry and deposition
909 on terrestrial bodies, *Environ. Sci. Pollut. Res.*, 20(11), 8092–8131,
910 doi:10.1007/s11356-013-2051-9, 2013.
- 911 Boersma, K. F., Jacob, D. J., Bucselá, E. J., Perring, A. E., Dirksen, R., van der A, R.

912 J., Yantosca, R. M., Park, R. J., Wenig, M. O., Bertram, T. H. and Cohen, R. C.:
913 Validation of OMI tropospheric NO₂ observations during INTEX-B and application to
914 constrain NO_x emissions over the eastern United States and Mexico, *Atmos.*
915 *Environ.*, 42(19), 4480–4497, doi:10.1016/j.atmosenv.2008.02.004, 2008.

916 Bond, T. C., Doherty, S. J., Fahey, D. W., Forster, P. M., Berntsen, T., Deangelo, B.
917 J., Flanner, M. G., Ghan, S., Kärcher, B., Koch, D., Kinne, S., Kondo, Y., Quinn, P.
918 K., Sarofim, M. C., Schultz, M. G., Schulz, M., Venkataraman, C., Zhang, H., Zhang,
919 S., Bellouin, N., Guttikunda, S. K., Hopke, P. K., Jacobson, M. Z., Kaiser, J. W.,
920 Klimont, Z., Lohmann, U., Schwarz, J. P., Shindell, D., Storelvmo, T., Warren, S. G.
921 and Zender, C. S.: Bounding the role of black carbon in the climate system: A
922 scientific assessment, *J. Geophys. Res. Atmos.*, 118(11), 5380–5552,
923 doi:10.1002/jgrd.50171, 2013.

924 Bouwman, A. F., Lee, D. S., Asman, W. A. H., Dentener, F. J., Van Der Hoek, K. W.
925 and Olivier, J. G. J.: A global high-resolution emission inventory for ammonia, *Global*
926 *Biogeochem. Cycles*, 11(4), 561–587, doi:10.1029/97GB02266, 1997.

927 Cao, H., Henze, D. K., Shephard, M. W., Dammers, E., Cady-Pereira, K., Alvarado,
928 M., Lonsdale, C., Luo, G., Yu, F., Zhu, L., Danielson, C. G. and Edgerton, E. S.:
929 Inverse modeling of NH₃ sources using CrIS remote sensing measurements,
930 *Environ. Res. Lett.*, in press, doi:10.1088/1748-9326/abb5cc, 2020.

931 Chen, Y., Morton, D. C., Jin, Y., Gollatz, G. J., Kasibhatla, P. S., Van Der Werf, G.
932 R., Defries, R. S. and Randerson, J. T.: Long-term trends and interannual variability
933 of forest, savanna and agricultural fires in South America, *Carbon Manag.*, 4(6), 617–
934 638, doi:10.4155/cmt.13.61, 2013.

935 Clarisse, L., Clerbaux, C., Dentener, F., Hurtmans, D. and Coheur, P.-F.: Global
936 ammonia distribution derived from infrared satellite observations, *Nat. Geosci.*, 2(7),
937 479–483 [online] Available from: <http://dx.doi.org/10.1038/ngeo551>, 2009.

938 Clarisse, L., Shephard, M. W., Dentener, F., Hurtmans, D., Cady-Pereira, K.,
939 Karagulian, F., Van Damme, M., Clerbaux, C. and Coheur, P. F.: Satellite monitoring
940 of ammonia: A case study of the San Joaquin Valley, *J. Geophys. Res.*, 115,
941 doi:10.1029/2009jd013291, 2010.

942 Clerbaux, C., Boynard, A., Clarisse, L., George, M., Hadji-Lazaro, J., Herbin, H.,
943 Hurtmans, D., Pommier, M., Razavi, A., Turquety, S., Wespes, C. and Coheur, P.-F.:
944 Monitoring of atmospheric composition using the thermal infrared IASI/MetOp
945 sounder, *Atmos. Chem. Phys.*, 9(16), 6041–6054, doi:10.5194/acp-9-6041-2009,
946 2009.

947 De Cort, M., Dubois, G., Fridman, S. D., Germenchuk, M., G., Izrael, Y. A., Janssens,
948 A., Jones, A. R., Kelly, G., N., Kvasnikova, E., V., Matveenko, I., I., Nazarov, I., N.,
949 Pokumeiko, Y., M., Sitak, V. A., Stukin, E., D., Tabachny, L., Y., Tsaturov, Y. S. and
950 Avdyushin, S., I.: Atlas of caesium deposition on Europe after the Chernobyl
951 accident, EU - Office for Official Publications of the European Communities,
952 Luxembourg., 1998.

953 Crippa, M., Janssens-Maenhout, G., Dentener, F., Guizzardi, D., Sindelarova, K.,
954 Muntean, M., Van Dingenen, R. and Granier, C.: Forty years of improvements in
955 European air quality: Regional policy-industry interactions with global impacts,
956 *Atmos. Chem. Phys.*, 16(6), 3825–3841, doi:10.5194/acp-16-3825-2016, 2016.

957 Croft, B., Pierce, J. R. and Martin, R. V.: Interpreting aerosol lifetimes using the
958 GEOS-Chem model and constraints from radionuclide measurements, *Atmos. Chem.*
959 *Phys.*, 14(8), 4313–4325, doi:10.5194/acp-14-4313-2014, 2014.

960 Van Damme, M., Wichink Kruit, R. J., Schaap, M., Clarisse, L., Clerbaux, C., Coheur,
961 P. F., Dammers, E., Dolman, A. J. and Erisman, J. W.: Evaluating 4 years of

962 atmospheric ammonia (NH₃) over Europe using IASI satellite observations and
 963 LOTOS-EUROS model results, *J. Geophys. Res. Atmos.*, 119(15), 9549–9566,
 964 doi:10.1002/2014JD021911, 2014a.
 965 Van Damme, M., Clarisse, L., Heald, C. L., Hurtmans, D., Ngadi, Y., Clerbaux, C.,
 966 Dolman, A. J., Erisman, J. W. and Coheur, P. F.: Global distributions, time series and
 967 error characterization of atmospheric ammonia (NH₃) from IASI satellite
 968 observations, *Atmos. Chem. Phys.*, 14(6), 2905–2922, doi:10.5194/acp-14-2905-
 969 2014, 2014b.
 970 Van Damme, M., Clarisse, L., Dammers, E., Liu, X., Nowak, J. B., Clerbaux, C.,
 971 Flechard, C. R., Galy-Lacaux, C., Xu, W., Neuman, J. A., Tang, Y. S., Sutton, M. A.,
 972 Erisman, J. W. and Coheur, P. F.: Towards validation of ammonia (NH₃)
 973 measurements from the IASI satellite, *Atmos. Meas. Tech.*, 8(3), 1575–1591,
 974 doi:10.5194/amt-8-1575-2015, 2015.
 975 Van Damme, M., Whitburn, S., Clarisse, L., Clerbaux, C., Hurtmans, D. and Coheur,
 976 P.: Version 2 of the IASI NH₃ neural network retrieval algorithm : near-real-time and
 977 reanalysed datasets, , 4905–4914, 2017.
 978 Van Damme, M., Clarisse, L., Whitburn, S., Hadji-Lazaro, J., Hurtmans, D., Clerbaux,
 979 C. and Coheur, P.-F.: Industrial and agricultural ammonia point sources exposed,
 980 *Nature*, 564(7734), 99–103, doi:10.1038/s41586-018-0747-1, 2018.
 981 Dammers, E., Palm, M., Van Damme, M., Vigouroux, C., Smale, D., Conway, S.,
 982 Toon, G. C., Jones, N., Nussbaumer, E., Warneke, T., Petri, C., Clarisse, L.,
 983 Clerbaux, C., Hermans, C., Lutsch, E., Strong, K., Hannigan, J. W., Nakajima, H.,
 984 Morino, I., Herrera, B., Stremme, W., Grutter, M., Schaap, M., Kruit, R. J. W., Notholt,
 985 J., Coheur, P. F. and Erisman, J. W.: An evaluation of IASI-NH₃ with ground-based
 986 Fourier transform infrared spectroscopy measurements, *Atmos. Chem. Phys.*,
 987 16(16), 10351–10368, doi:10.5194/acp-16-10351-2016, 2016.
 988 Dammers, E., Shephard, M. W., Palm, M., Cady-pereira, K., Capps, S., Lutsch, E.,
 989 Strong, K., Hannigan, J. W., Ortega, I., Toon, G. C., Stremme, W. and Grutter, M.:
 990 Validation of the CrIS fast physical NH₃ retrieval with ground-based FTIR, , 87,
 991 2645–2667, 2017.
 992 Dammers, E., McLinden, C. A., Griffin, D., Shephard, M. W., Van Der Graaf, S.,
 993 Lutsch, E., Schaap, M., Gainairu-Matz, Y., Fioletov, V., Van Damme, M., Whitburn,
 994 S., Clarisse, L., Cady-Pereira, K., Clerbaux, C., Francois Coheur, P. and Erisman, J.
 995 W.: NH₃ emissions from large point sources derived from CrIS and IASI satellite
 996 observations, *Atmos. Chem. Phys.*, 19(19), 12261–12293, doi:10.5194/acp-19-
 997 12261-2019, 2019.
 998 Datta, A., Sharma, S. K., Harit, R. C., Kumar, V., Mandal, T. K. and Pathak, H.:
 999 Ammonia emission from subtropical crop land area in india, *Asia-Pacific J. Atmos.*
 1000 *Sci.*, 48(3), 275–281, doi:10.1007/s13143-012-0027-1, 2012.
 1001 Dee, D. P., Uppala, S. M., Simmons, A. J., Berrisford, P., Poli, P., Kobayashi, S.,
 1002 Andrae, U., Balmaseda, M. A., Balsamo, G., Bauer, P., Bechtold, P., Beljaars, A. C.
 1003 M., van de Berg, L., Bidlot, J., Bormann, N., Delsol, C., Dragani, R., Fuentes, M.,
 1004 Geer, A. J., Haimberger, L., Healy, S. B., Hersbach, H., H??lm, E. V., Isaksen, L.,
 1005 K??llberg, P., K??hler, M., Matricardi, M., McNally, A. P., Monge-Sanz, B. M.,
 1006 Morcrette, J. J., Park, B. K., Peubey, C., de Rosnay, P., Tavolato, C., Th??paut, J. N.
 1007 and Vitart, F.: The ERA-Interim reanalysis: Configuration and performance of the
 1008 data assimilation system, *Q. J. R. Meteorol. Soc.*, 137(656), 553–597,
 1009 doi:10.1002/qj.828, 2011.
 1010 Dentener, F. J. and Crutzen, P. J.: A 3-Dimensional Model Of The Global Ammonia
 1011 Cycle, *J. Atmos. Chem.*, 19(4), 331–369, doi:10.1007/bf00694492, 1994.

1012 Duncan, B. N., Lamsal, L. N., Thompson, A. M., Yoshida, Y., Lu, Z., Streets, D. G.,
1013 Hurwitz, M. M. and Pickering, K. E.: A space-based, high-resolution view of notable
1014 changes in urban NO_x pollution around the world (2005–2014), *J. Geophys. Res.*
1015 *Ocean.*, 121, 976–996, doi:10.1002/2015JD024121, 2016.
1016 Elissavet Koukouli, M., Theys, N., Ding, J., Zyrichidou, I., Mijling, B., Balis, D. and
1017 Johannes Van Der A, R.: Updated SO₂ emission estimates over China using
1018 OMI/Aura observations, *Atmos. Meas. Tech.*, 11(3), 1817–1832, doi:10.5194/amt-11-
1019 1817-2018, 2018.
1020 Emanuel, K. A.: A Scheme for Representing Cumulus Convection in Large-Scale
1021 Models, *J. Atmos. Sci.*, 48(21), 2313–2329, doi:10.1175/1520-
1022 0469(1991)048<2313:ASFRCC>2.0.CO;2, 1991.
1023 Erisman, J. A. N. W.: The Nanjing Declaration on Management of Reactive Nitrogen,
1024 *J. Atmos. Sci.*, 54(4), 286–287, 2004.
1025 Erisman, J. W., Bleeker, A., Galloway, J. and Sutton, M. S.: Reduced nitrogen in
1026 ecology and the environment, *Environ. Pollut.*, 150(1), 140–149,
1027 doi:10.1016/j.envpol.2007.06.033, 2007.
1028 Escobar, H.: Amazon fires clearly linked to deforestation, scientists say, *Science* (80-
1029 .), 365(6456), 853, doi:10.1126/science.365.6456.853, 2019.
1030 European Environment Agency: EMEP/EEA air pollutant emission inventory
1031 guidebook 2019: Technical guidance to prepare national emission inventories., 2019.
1032 Evangeliou, N., Hamburger, T., Talerko, N., Zibtsev, S., Bondar, Y., Stohl, A.,
1033 Balkanski, Y., Mousseau, T. A. and Møller, A. P.: Reconstructing the Chernobyl
1034 Nuclear Power Plant (CNPP) accident 30 years after. A unique database of air
1035 concentration and deposition measurements over Europe, *Environ. Pollut.*, (August),
1036 doi:10.1016/j.envpol.2016.05.030, 2016.
1037 Faulkner, W. B. and Shaw, B. W.: Review of ammonia emission factors for United
1038 States animal agriculture, *Atmos. Environ.*, 42(27), 6567–6574,
1039 doi:10.1016/j.atmosenv.2008.04.021, 2008.
1040 Flechard, C. R. and Fowler, D.: Atmospheric ammonia at a moorland site. I: The
1041 meteorological control of ambient ammonia concentrations and the influence of local
1042 sources, *Q. J. R. Meteorol. Soc.*, 124(547), 733–757, doi:10.1256/smsqj.54704,
1043 1998.
1044 Folberth, G. A., Hauglustaine, D. A., Lathière, J. and Brocheton, F.: Interactive
1045 chemistry in the Laboratoire de Météorologie Dynamique general circulation model:
1046 model description and impact analysis of biogenic hydrocarbons on tropospheric
1047 chemistry, *Atmos. Chem. Phys.*, 6(8), 2273–2319, doi:10.5194/acp-6-2273-2006,
1048 2006.
1049 Fowler, D., Muller, J. B. A., Smith, R. I., Dragosits, U., Skiba, U., Sutton, M. A. and
1050 Brimblecombe, P.: A CHRONOLOGY OF NITROGEN DEPOSITION IN THE UK, , 2,
1051 9–23, 2004.
1052 Gelaro, R., McCarty, W., Suárez, M. J., Todling, R., Molod, A., Takacs, L., Randles,
1053 C. A., Darmenov, A., Bosilovich, M. G., Reichle, R., Wargan, K., Coy, L., Cullather,
1054 R., Draper, C., Akella, S., Buchard, V., Conaty, A., da Silva, A. M., Gu, W., Kim, G.
1055 K., Koster, R., Lucchesi, R., Merkova, D., Nielsen, J. E., Partyka, G., Pawson, S.,
1056 Putman, W., Rienecker, M., Schubert, S. D., Sienkiewicz, M. and Zhao, B.: The
1057 modern-era retrospective analysis for research and applications, version 2 (MERRA-
1058 2), *J. Clim.*, 30(14), 5419–5454, doi:10.1175/JCLI-D-16-0758.1, 2017.
1059 Giglio, L., Randerson, J. T. and van der Werf, G. R.: Analysis of daily, monthly, and
1060 annual burned area using the fourth-generation global fire emissions database
1061 (GFED4), *J. Geophys. Res. Biogeosciences*, 118, 317–328, doi:10.1002/jgrg.20042,

1062 2013, 2013.
1063 Gu, B., Sutton, M. A., Chang, S. X., Ge, Y. and Chang, J.: Agricultural ammonia
1064 emissions contribute to China's urban air pollution, *Front. Ecol. Environ.*, 12(5), 265–
1065 266, doi:10.1890/14.WB.007, 2014.
1066 Hauglustaine, D. A., Hourdin, F., Jourdain, L., Filiberti, M.-A., Walters, S., Lamarque,
1067 J.-F. and Holland, E. A.: Interactive chemistry in the Laboratoire de Meteorologie
1068 Dynamique general circulation model: Description and background tropospheric
1069 chemistry evaluation, *J. Geophys. Res.*, 109(D04314), doi:10.1029/2003JD003957,
1070 2004.
1071 Hauglustaine, D. A., Balkanski, Y. and Schulz, M.: A global model simulation of
1072 present and future nitrate aerosols and their direct radiative forcing of climate, *Atmos.*
1073 *Chem. Phys.*, 14(20), 11031–11063, doi:10.5194/acp-14-11031-2014, 2014.
1074 Henze, D. K., Shindell, D. T., Akhtar, F., Spurr, R. J. D., Pinder, R. W., Loughlin, D.,
1075 Kopacz, M., Singh, K. and Shim, C.: Spatially Refined Aerosol Direct Radiative
1076 Forcing Efficiencies, *Environ. Sci. Technol.*, 46, 9511–9518, doi:10.1021/es301993s,
1077 2012.
1078 Hertel, O., Skjoth, C. A., Reis, S., Bleeker, A., Harrison, R. M., Cape, J. N., Fowler,
1079 D., Skiba, U., Simpson, D., Jickells, T., Kulmala, M., Gyldenkerne, S., Sorensen, L.
1080 L., Erisman, J. W. and Sutton, M. A.: Governing processes for reactive nitrogen
1081 compounds in the European atmosphere, *Biogeosciences*, 9(12), 4921–4954,
1082 doi:10.5194/bg-9-4921-2012, 2012.
1083 Hourdin, F. and Armengaud, A.: The Use of Finite-Volume Methods for Atmospheric
1084 Advection of Trace Species. Part I: Test of Various Formulations in a General
1085 Circulation Model, *Mon. Weather Rev.*, 127(5), 822–837, doi:10.1175/1520-
1086 0493(1999)127<0822:TUOFVM>2.0.CO;2, 1999.
1087 Hourdin, F., Musat, I., Bony, S., Braconnot, P., Codron, F., Dufresne, J. L., Fairhead,
1088 L., Filiberti, M. A., Friedlingstein, P., Grandpeix, J. Y., Krinner, G., LeVan, P., Li, Z. X.
1089 and Lott, F.: The LMDZ4 general circulation model: Climate performance and
1090 sensitivity to parametrized physics with emphasis on tropical convection, *Clim. Dyn.*,
1091 27(7–8), 787–813, doi:10.1007/s00382-006-0158-0, 2006.
1092 Hov, Ø., Hjøllø, B. A. and Eliassen, A.: Transport distance of ammonia and
1093 ammonium in Northern Europe: 2. Its relation to emissions of SO₂ and NO_x, *J.*
1094 *Geophys. Res.*, 99(D9), 18749, doi:10.1029/94jd00910, 1994.
1095 Kajino, M., Ueda, H., Satsumabayashi, H. and An, J.: Impacts of the eruption of
1096 Miyakejima Volcano on air quality over far east Asia, *J. Geophys. Res. D Atmos.*,
1097 109(21), 1–11, doi:10.1029/2004JD004762, 2004.
1098 Kean, A. J., Littlejohn, D., Ban-Weiss, G. A., Harley, R. A., Kirchstetter, T. W. and
1099 Lunden, M. M.: Trends in on-road vehicle emissions of ammonia, *Atmos. Environ.*,
1100 43(8), 1565–1570, doi:10.1016/j.atmosenv.2008.09.085, 2009.
1101 Kharol, S. K., Shephard, M. W., McLinden, C. A., Zhang, L., Sioris, C. E., O'Brien, J.
1102 M., Vet, R., Cady-Pereira, K. E., Hare, E., Siemons, J. and Krotkov, N. A.: Dry
1103 Deposition of Reactive Nitrogen From Satellite Observations of Ammonia and
1104 Nitrogen Dioxide Over North America, *Geophys. Res. Lett.*, 45(2), 1157–1166,
1105 doi:10.1002/2017GL075832, 2018.
1106 Klimont, Z., Kupiainen, K., Heyes, C., Purohit, P., Cofala, J., Rafaj, P., Borken-
1107 Kleefeld, J. and Schöpp, W.: Global anthropogenic emissions of particulate matter
1108 including black carbon, *Atmos. Chem. Phys.*, 17, 8681–8723, doi:10.5194/acp-17- 50
1109 8681-2017, 2017.
1110 Krinner, G., Viovy, N., de Noblet-Ducoudré, N., Ogée, J., Polcher, J., Friedlingstein,
1111 P., Ciais, P., Sitch, S. and Prentice, I. C.: A dynamic global vegetation model for

1112 studies of the coupled atmosphere-biosphere system, *Global Biogeochem. Cycles*,
1113 19(1), n/a--n/a, doi:10.1029/2003GB002199, 2005.

1114 Krotkov, N. A., McLinden, C. A., Li, C., Lamsal, L. N., Celarier, E. A., Marchenko, S.
1115 V., Swartz, W. H., Bucsela, E. J., Joiner, J., Duncan, B. N., Folkert Boersma, K.,
1116 Pepijn Veefkind, J., Levelt, P. F., Fioletov, V. E., Dickerson, R. R., He, H., Lu, Z. and
1117 Streets, D. G.: Aura OMI observations of regional SO₂ and NO₂ pollution changes
1118 from 2005 to 2015, *Atmos. Chem. Phys.*, 16(7), 4605–4629, doi:10.5194/acp-16-
1119 4605-2016, 2016.

1120 Kuttippurath, J., Singh, A., Dash, S. P., Mallick, N., Clerbaux, C., Van Damme, M.,
1121 Clarisse, L., Coheur, P. F., Raj, S., Abhishek, K. and Varikoden, H.: Record high
1122 levels of atmospheric ammonia over India: Spatial and temporal analyses, *Sci. Total*
1123 *Environ.*, 740, 139986, doi:10.1016/j.scitotenv.2020.139986, 2020.

1124 Lachatre, M., Fortems-Cheiney, A., Foret, G., Siour, G., Dufour, G., Clarisse, L.,
1125 Clerbaux, C., Coheur, P. F., Van Damme, M. and Beekmann, M.: The unintended
1126 consequence of SO₂ and NO₂ regulations over China: Increase of ammonia levels
1127 and impact on PM_{2.5} concentrations, *Atmos. Chem. Phys.*, 19(10), 6701–6716,
1128 doi:10.5194/acp-19-6701-2019, 2019.

1129 Leip, A., Billen, G., Garnier, J., Grizzetti, B., Lassaletta, L., Reis, S., Simpson, D.,
1130 Sutton, M. a, de Vries, W., Weiss, F. and Westhoek, H.: Impacts of European
1131 livestock production: nitrogen, sulphur, phosphorus and greenhouse gas emissions,
1132 land-use, water eutrophication and biodiversity, *Environ. Res. Lett.*, 10(11), 115004,
1133 doi:10.1088/1748-9326/10/11/115004, 2015.

1134 Lelieveld, J., Evans, J. S., Fnais, M., Giannadaki, D. and Pozzer, A.: The contribution
1135 of outdoor air pollution sources to premature mortality on a global scale., *Nature*,
1136 525(7569), 367–71, doi:10.1038/nature15371, 2015.

1137 Li, C., Martin, R. V., Shephard, M. W., Pereira, K. C., Cooper, M. J., Kaiser, J., Lee,
1138 C. J., Zhang, L. and Henze, D. K.: Assessing the Iterative Finite Difference Mass
1139 Balance and 4D - Var Methods to Derive Ammonia Emissions Over North America
1140 Using Synthetic Observations, , 4222–4236, doi:10.1029/2018JD030183, 2019.

1141 Lin, J. T., McElroy, M. B. and Boersma, K. F.: Constraint of anthropogenic NO_x
1142 emissions in China from different sectors: A new methodology using multiple satellite
1143 retrievals, *Atmos. Chem. Phys.*, 10(1), 63–78, doi:10.5194/acp-10-63-2010, 2010.

1144 Liu, F., Beirle, S., Zhang, Q., van der A, R. J., Zheng, B., Tong, D. and He, K.: NO_x
1145 emission trends over Chinese cities estimated from OMI observations during 2005 to
1146 2015, *Atmos. Chem. Phys. Discuss.*, (2), 1–21, doi:10.5194/acp-2017-369, 2017.

1147 Liu, L., Zhang, X., Wong, A. Y. H., Xu, W., Liu, X., Li, Y., Mi, H., Lu, X., Zhao, L.,
1148 Wang, Z. and Wu, X.: Estimating global surface ammonia concentrations inferred
1149 from satellite retrievals, *Atmos. Chem. Phys.*, (19), 12051–12066, doi:10.5194/acp-
1150 19-12051-2019, 2019.

1151 Liu, M., Huang, X., Song, Y., Xu, T., Wang, S., Wu, Z., Hu, M., Zhang, L., Zhang, Q.,
1152 Pan, Y. and Zhu, T.: Rapid SO₂ emission reductions significantly increase
1153 tropospheric ammonia concentrations over the North China Plain, *Atmos. Chem.*
1154 *Phys.*, (18), 17933–17943, doi:10.5194/acp-18-17933-2018, 2018.

1155 Makar, P. A., Moran, M. D., Zheng, Q., Cousineau, S., Sassi, M., Duhamel, A.,
1156 Besner, M., Davignon, D., Crevier, L. P. and Bouchet, V. S.: Modelling the impacts of
1157 ammonia emissions reductions on North American air quality, *Atmos. Chem. Phys.*,
1158 9(18), 7183–7212, doi:10.5194/acp-9-7183-2009, 2009.

1159 Malm, W. C.: Spatial and monthly trends in speciated fine particle concentration in
1160 the United States, *J. Geophys. Res.*, 109(D3), D03306, doi:10.1029/2003JD003739,
1161 2004.

1162 Malm, W. C., Schichtel, B. A., Barna, M. G., Gebhart, K. A., Rodriguez, M. A., Collett,
1163 J. L., Carrico, C. M., Benedict, K. B., Prenni, A. J. and Kreidenweis, S. M.: Aerosol
1164 species concentrations and source apportionment of ammonia at Rocky Mountain
1165 National Park, *J. Air Waste Manag. Assoc.*, 63(11), 1245–1263,
1166 doi:10.1080/10962247.2013.804466, 2013.
1167 van Marle, M. J. E., Field, R. D., van der Werf, G. R., Estrada de Wagt, I. A.,
1168 Houghton, R. A., Rizzo, L. V., Artaxo, P. and Tsigaridis, K.: Fire and deforestation
1169 dynamics in Amazonia (1973–2014), *Global Biogeochem. Cycles*, 31(1), 24–38,
1170 doi:10.1002/2016GB005445, 2017.
1171 McQuilling, A. M.: Ammonia emissions from livestock in the United States: From farm
1172 emissions models to a new national inventory, ProQuest Diss. Theses, 168 [online]
1173 Available from:
1174 [https://search.proquest.com/docview/1841254436?accountid=133571%0Ahttp://www](https://search.proquest.com/docview/1841254436?accountid=133571%0Ahttp://www.yidu.edu.cn/educhina/educhina.do?artifact=&svalue=Ammonia+emissions+from+live+stock+in+the+United+States%3A+From+farm+emissions+models+to+a+new+national+inventory&stype=2&s=on%0Ah)
1175 [.yidu.edu.cn/educhina/educhina.do?artifact=&svalue=Ammonia+emissions+from+live](https://search.proquest.com/docview/1841254436?accountid=133571%0Ahttp://www.yidu.edu.cn/educhina/educhina.do?artifact=&svalue=Ammonia+emissions+from+live+stock+in+the+United+States%3A+From+farm+emissions+models+to+a+new+national+inventory&stype=2&s=on%0Ah)
1176 [stock+in+the+United+States%3A+From+farm+emissions+models+to+a+new+nation](https://search.proquest.com/docview/1841254436?accountid=133571%0Ahttp://www.yidu.edu.cn/educhina/educhina.do?artifact=&svalue=Ammonia+emissions+from+live+stock+in+the+United+States%3A+From+farm+emissions+models+to+a+new+national+inventory&stype=2&s=on%0Ah)
1177 [al+inventory&stype=2&s=on%0Ah](https://search.proquest.com/docview/1841254436?accountid=133571%0Ahttp://www.yidu.edu.cn/educhina/educhina.do?artifact=&svalue=Ammonia+emissions+from+live+stock+in+the+United+States%3A+From+farm+emissions+models+to+a+new+national+inventory&stype=2&s=on%0Ah), 2016.
1178 Min Hao, W., Petkov, A., Nordgren, B. L., Corley, R. E., Silverstein, R. P., Urbanski,
1179 S. P., Evangelidou, N., Balkanski, Y. and Kinder, B. L.: Daily black carbon emissions
1180 from fires in northern Eurasia for 2002-2015, *Geosci. Model Dev.*, 9(12),
1181 doi:10.5194/gmd-9-4461-2016, 2016.
1182 Möller, D. and Schieferdecker, H.: A relationship between agricultural NH₃
1183 emissions and the atmospheric SO₂ content over industrial areas, *Atmos. Environ.*,
1184 19(5), 695–700, doi:10.1016/0004-6981(85)90056-3, 1985.
1185 Norman, M. and Leck, C.: Distribution of marine boundary layer ammonia over the
1186 Atlantic and Indian Oceans during the Aerosols99 cruise, *J. Geophys. Res. D*
1187 *Atmos.*, 110(16), 1–11, doi:10.1029/2005JD005866, 2005.
1188 Pan, Y., Tian, S., Zhao, Y., Zhang, L., Zhu, X., Gao, J., Huang, W., Zhou, Y., Song,
1189 Y., Zhang, Q. and Wang, Y.: Identifying Ammonia Hotspots in China Using a National
1190 Observation Network, *Environ. Sci. Technol.*, 52(7), 3926–3934,
1191 doi:10.1021/acs.est.7b05235, 2018.
1192 Parzen, E.: On the Estimation of Probability Density Functions and Mode, *Ann. Math.*
1193 *Stat.*, 33, 1065–1076, 1962.
1194 Paulot, F., Jacob, D. J., Pinder, R. W., Bash, J. O., Travis, K. and Henze, D. K.:
1195 Ammonia emissions in the United States, European Union, and China derived by
1196 high-resolution inversion of ammonium wet deposition data: Interpretation with a new
1197 agricultural emissions inventory (MASAGE-NH₃), *J. Geophys. Res. Atmos.*, 119(7),
1198 4343–4364, doi:10.1002/2013JD021130, 2014.
1199 Pinder, R. W., Gilliland, A. B. and Dennis, R. L.: Environmental impact of
1200 atmospheric NH₃ emissions under present and future conditions in the
1201 eastern United States, *Geophys. Res. Lett.*, 35(12), 1–6,
1202 doi:10.1029/2008GL033732, 2008.
1203 Pope III, C. A., Burnett, R. T., Thun, M. J., Calle, E. E., Krewski, D. and Thurston, G.
1204 D.: Lung Cancer, Cardiopulmonary Mortality, and Long-term Exposure to Fine
1205 Particulate Air Pollution, *J. Am. Med. Assoc.*, 287(9), 1132–1141,
1206 doi:10.1001/jama.287.9.1132, 2002.
1207 Quinn, P. K., Bates, T. S. and Johnson, J. E.: Interactions Between the Sulfur and
1208 Reduced Nitrogen Cycles Over the Central Pacific Ocean, *J. Geophys. Res.*,
1209 95(D10), 16405–16416, 1990.
1210 R'Honi, Y., Clarisse, L., Clerbaux, C., Hurtmans, D., Dufлот, V., Turquety, S., Ngadi,
1211 Y. and Coheur, P. F.: Exceptional emissions of NH₃ and HCOOH in the 2010

1212 Russian wildfires, *Atmos. Chem. Phys.*, 13(1), 4171–4181, doi:10.5194/acp-13-4171-
1213 2013, 2013.

1214 Reche, C., Viana, M., Pandolfi, M., Alastuey, A., Moreno, T., Amato, F., Ripoll, A. and
1215 Querol, X.: Urban NH₃ levels and sources in a Mediterranean environment, *Atmos.*
1216 *Environ.*, 57, 153–164, doi:10.1016/j.atmosenv.2012.04.021, 2012.

1217 Reis, S., Pinder, R. W., Zhang, M., Lijie, G. and Sutton, M. A.: Reactive nitrogen in
1218 atmospheric emission inventories, *Atmos. Chem. Phys.*, 9(19), 7657–7677,
1219 doi:10.5194/acp-9-7657-2009, 2009.

1220 Renka, R. J.: Multivariate Interpolation of Large Sets of Scattered Data, *ACM Trans.*
1221 *Math. Softw.*, 14(2), 139–148, doi:10.1145/45054.45055, 1988.

1222 Schulz, M.: Constraining model estimates of the aerosol Radiative Forcing,
1223 Université Pierre et Marie Curie, Paris VI., 2007.

1224 Scott, D. W.: Multivariate density estimation: Theory, practice, and visualization:
1225 Second edition., 2015.

1226 Seinfeld, J. H. and Pandis, S. N.: *Atmospheric Chemistry and Physics. From Air*
1227 *Pollution to Climate Change*, 2nd ed., John Wiley & Sons, NY., 2000.

1228 Shephard, M. W. and Cady-Pereira, K. E.: Cross-track Infrared Sounder (CrIS)
1229 satellite observations of tropospheric ammonia, *Atmos. Meas. Tech.*, 8(3), 1323–
1230 1336, doi:10.5194/amt-8-1323-2015, 2015.

1231 Shephard, M. W., McLinden, C. A., Cady-Pereira, K. E., Luo, M., Moussa, S. G.,
1232 Leithead, A., Liggio, J., Staebler, R. M., Akingunola, A., Makar, P., Lehr, P., Zhang,
1233 J., Henze, D. K., Millet, D. B., Bash, J. O., Zhu, L., Wells, K. C., Capps, S. L.,
1234 Chaliyakunnel, S., Gordon, M., Hayden, K., Brook, J. R., Wolde, M. and Li, S. M.:
1235 Tropospheric Emission Spectrometer (TES) satellite observations of ammonia,
1236 methanol, formic acid, and carbon monoxide over the Canadian oil sands: Validation
1237 and model evaluation, *Atmos. Meas. Tech.*, 8(12), 5189–5211, doi:10.5194/amt-8-
1238 5189-2015, 2015.

1239 Shephard, M. W., Dammers, E., Cady-Pereira, K., Kharol, S., Thompson, J.,
1240 Gainariu-Matz, Y., Zhang, J., A. McLinden, C., Kovachik, A., Moran, M., Bittman, S.,
1241 E. Sioris, C., Griffin, D., J. Alvarado, M., Lonsdale, C., Savic-Jovicic, V. and Zheng,
1242 Q.: Ammonia measurements from space with the Cross-track Infrared Sounder:
1243 Characteristics and applications, *Atmos. Chem. Phys.*, 20(4), 2277–2302,
1244 doi:10.5194/acp-20-2277-2020, 2020.

1245 Someya, Y., Imasu, R., Shiomi, K. and Saitoh, N.: Atmospheric ammonia retrieval
1246 from the TANSO-FTS / GOSAT thermal infrared sounder, , 1990, 309–321, 2020.

1247 Sørensen, L. L., Hertel, O., Skjøth, C. A., Lund, M. and Pedersen, B.: Fluxes of
1248 ammonia in the coastal marine boundary layer, *Atmos. Environ.*, 37(SUPPL. 1), 167–
1249 177, doi:10.1016/S1352-2310(03)00247-4, 2003.

1250 Stevens, C. J., Dupr, C., Dorland, E., Gaudnik, C., Gowing, D. J. G., Bleeker, A.,
1251 Diekmann, M., Alard, D., Bobbink, R., Fowler, D., Corcket, E., Mountford, J. O.,
1252 Vandvik, V., Aarrestad, P. A., Muller, S. and Dise, N. B.: Nitrogen deposition
1253 threatens species richness of grasslands across Europe, *Environ. Pollut.*, 158(9),
1254 2940–2945, doi:10.1016/j.envpol.2010.06.006, 2010.

1255 Streets, D. G., Canty, T., Carmichael, G. R., de Foy, B., Dickerson, R. R., Duncan, B.
1256 N., Edwards, D. P., Haynes, J. A., Henze, D. K., Houyoux, M. R., Jacob, D. J.,
1257 Krotkov, N. A., Lamsal, L. N., Liu, Y., Lu, Z., Martin, R. V, Pfister, G. G., Pinder, R.
1258 W., Salawitch, R. J. and Wecht, K. J.: Emissions estimation from satellite retrievals: A
1259 review of current capability, *Atmos. Environ.*, 77, 1011–1042,
1260 doi:https://doi.org/10.1016/j.atmosenv.2013.05.051, 2013.

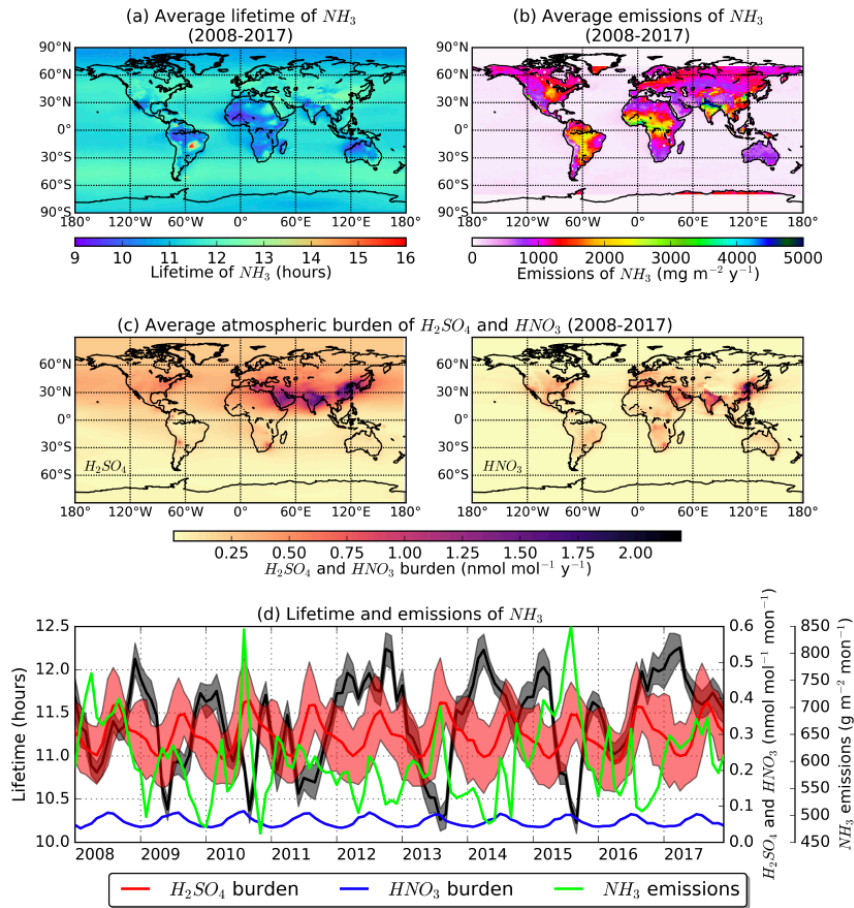
1261 Sutton, M. A., Fowler, D., Moncrieff, J. B. and Storeton-West, R. L.: The exchange of

1262 atmospheric ammonia with vegetated surfaces. II: Fertilized vegetation, Q. J. R.
1263 Meteorol. Soc., 119(513), 1047–1070, doi:10.1002/qj.49711951310, 1993.
1264 Sutton, M. A., Dragosits, U., Tang, Y. S. and Fowler, D.: Ammonia emissions from
1265 non-agricultural sources in the UK, , 34(August 1999), 2000.
1266 Sutton, M. A., Erisman, J. W., Dentener, F. and Möller, D.: Ammonia in the
1267 environment: From ancient times to the present, Environ. Pollut., 156(3), 583–604,
1268 doi:10.1016/j.envpol.2008.03.013, 2008.
1269 Tanvir, A., Khokhar, M. F., Javed, Z., Sandhu, O., Mustansar, T. and Shoaib, A.:
1270 Spatiotemporal evolution of atmospheric ammonia columns over the indo-gangetic
1271 plain by exploiting satellite observations, Adv. Meteorol., 2019,
1272 doi:10.1155/2019/7525479, 2019.
1273 Turner, A. J., Henze, D. K., Martin, R. V. and Hakami, A.: The spatial extent of
1274 source influences on modeled column concentrations of short-lived species,
1275 Geophys. Res. Lett., 39(12), 1–5, doi:10.1029/2012GL051832, 2012.
1276 Uematsu, M., Toratani, M., Kajino, M., Narita, Y., Senga, Y. and Kimoto, T.:
1277 Enhancement of primary productivity in the western North Pacific caused by the
1278 eruption of the Miyake-jima Volcano, Geophys. Res. Lett., 31(6), n/a-n/a,
1279 doi:10.1029/2003gl018790, 2004.
1280 Vincenty, T.: Direct and inverse solutions of geodesics on the ellipsoid with
1281 application of nested equations, Surv. Rev. XXIII (misprinted as XXII), 176, 88–93,
1282 1975.
1283 De Vries, W., Kros, J., Reinds, G. J. and Butterbach-Bahl, K.: Quantifying impacts of
1284 nitrogen use in European agriculture on global warming potential, Curr. Opin.
1285 Environ. Sustain., 3(5), 291–302, doi:10.1016/j.cosust.2011.08.009, 2011.
1286 Wang, Y., Zhang, Q. Q., He, K., Zhang, Q. and Chai, L.: Sulfate-nitrate-ammonium
1287 aerosols over China: Response to 2000-2015 emission changes of sulfur dioxide,
1288 nitrogen oxides, and ammonia, Atmos. Chem. Phys., 13(5), 2635–2652,
1289 doi:10.5194/acp-13-2635-2013, 2013.
1290 Warner, J. X., Dickerson, R. R., Wei, Z., Strow, L. L., Wang, Y. and Liang, Q.:
1291 Increased atmospheric ammonia over the world's major agricultural areas detected
1292 from space, Geophys. Res. Lett., 1–10, doi:10.1002/2016GL072305, 2017.
1293 Webb, J., Menzi, H., Pain, B. F., Misselbrook, T. H., Dämmgen, U., Hendriks, H. and
1294 Döhler, H.: Managing ammonia emissions from livestock production in Europe,
1295 Environ. Pollut., 135(3 SPEC. ISS.), 399–406, doi:10.1016/j.envpol.2004.11.013,
1296 2005.
1297 Whitburn, S., Van Damme, M., Kaiser, J. W., Van Der Werf, G. R., Turquety, S.,
1298 Hurtmans, D., Clarisse, L., Clerbaux, C. and Coheur, P. F.: Ammonia emissions in
1299 tropical biomass burning regions: Comparison between satellite-derived emissions
1300 and bottom-up fire inventories, Atmos. Environ., 121, 42–54,
1301 doi:10.1016/j.atmosenv.2015.03.015, 2014.
1302 Whitburn, S., Van Damme, M., Clarisse, L., Bauduin, S., Heald, C. L., Hadji-Lazaro,
1303 J., Hurtmans, D., Zondlo, M. A., Clerbaux, C. and Coheur, P. F.: A flexible and robust
1304 neural network IASI-NH₃ retrieval algorithm, J. Geophys. Res., 121(11), 6581–6599,
1305 doi:10.1002/2016JD024828, 2016a.
1306 Whitburn, S., Damme, M. Van, Clarisse, L., Turquety, S., Clerbaux, C. and Coheur,
1307 P. -: Peat fires doubled annual ammonia emissions in Indonesia during the 2015 El
1308 Niño, Geophys. Res. Lett., doi:10.1002/2016GL070620, 2016b.
1309 Xu, L. and Penner, J. E.: Global simulations of nitrate and ammonium aerosols and
1310 their radiative effects, Atmos. Chem. Phys., 12(20), 9479–9504, doi:10.5194/acp-12-
1311 9479-2012, 2012.

1312 Xu, P., Liao, Y. J., Lin, Y. H., Zhao, C. X., Yan, C. H., Cao, M. N., Wang, G. S. and
1313 Luan, S. J.: High-resolution inventory of ammonia emissions from agricultural
1314 fertilizer in China from 1978 to 2008, *Atmos. Chem. Phys.*, 16(3), 1207–1218,
1315 doi:10.5194/acp-16-1207-2016, 2016.
1316 Xu, R. T., Pan, S. F., Chen, J., Chen, G. S., Yang, J., Dangal, S. R. S., Shepard, J.
1317 P. and Tian, H. Q.: Half-Century Ammonia Emissions From Agricultural Systems in
1318 Southern Asia: Magnitude, Spatiotemporal Patterns, and Implications for Human
1319 Health, *GeoHealth*, 2(1), 40–53, doi:10.1002/2017gh000098, 2018.
1320 Yang, K., Krotkov, N. A., Krueger, A. J., Carn, S. A., Bhartia, P. K. and Levelt, P. F.:
1321 Retrieval of large volcanic SO₂ columns from the Aura Ozone Monitoring
1322 Instrument: Comparison and limitations, *J. Geophys. Res. Atmos.*, 112(24), 1–14,
1323 doi:10.1029/2007JD008825, 2007.
1324 Zavyalov, V., Esplin, M., Scott, D., Esplin, B., Bingham, G., Hoffman, E., Lietzke, C.,
1325 Predina, J., Frain, R., Suwinski, L., Han, Y., Major, C., Graham, B. and Phillips, L.:
1326 Noise performance of the CrIS instrument, , 118, 108–120,
1327 doi:10.1002/2013JD020457, 2013.
1328 Zhao, C. and Wang, Y.: Assimilated inversion of NO_x emissions over east Asia using
1329 OMINO₂ column measurements, *Geophys. Res. Lett.*, 36(6), 1–5,
1330 doi:10.1029/2008GL037123, 2009.
1331 Zhu, L., Henze, D. K., Cady-Pereira, K. E., Shephard, M. W., Luo, M., Pinder, R. W.,
1332 Bash, J. O. and Jeong, G. R.: Constraining U.S. ammonia emissions using TES
1333 remote sensing observations and the GEOS-Chem adjoint model, *J. Geophys. Res.*
1334 *Atmos.*, 118(8), 3355–3368, doi:10.1002/jgrd.50166, 2013.
1335 Zhu, L., Henze, D. K., Bash, J. O., Cady-Pereira, K. E., Shephard, M. W., Luo, M.
1336 and Capps, S. L.: Sources and Impacts of Atmospheric NH₃: Current Understanding
1337 and Frontiers for Modeling, Measurements, and Remote Sensing in North America,
1338 *Curr. Pollut. Reports*, 1(2), 95–116, doi:10.1007/s40726-015-0010-4, 2015.
1339
1340

1341 FIGURE LEGENDS

1342



1343

1344

1345

1346

1347

1348

Figure 1. (a) 10-year average model lifetime of ammonia calculated from the LMDz-OR-INCA, (b) total annual emissions averaged over the 10-year period (NE emissions), (c) atmospheric burden of the reactants sulfuric and nitric acid calculated in the model, and (d) monthly timeseries of lifetime (black), ammonia emissions (green), sulfuric (red) and nitric acid column concentrations (blue) for the whole 10-year period.

1349

(a) Average lifetime of NH_3 (2008-2017)

(b) Average emissions of NH_3 (2008-2017)

(c) Average atmospheric burden of H_2SO_4 and HNO_3 (2008-2017)

(d) Lifetime and emissions of NH_3

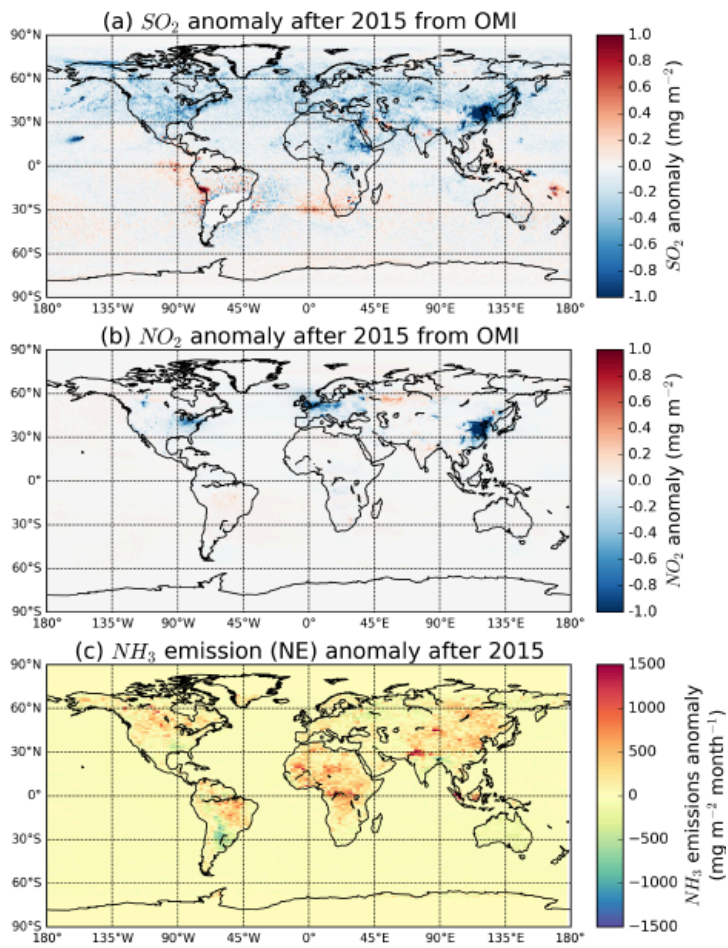
Deleted:

Deleted: A

Deleted: model

Deleted: sulfate

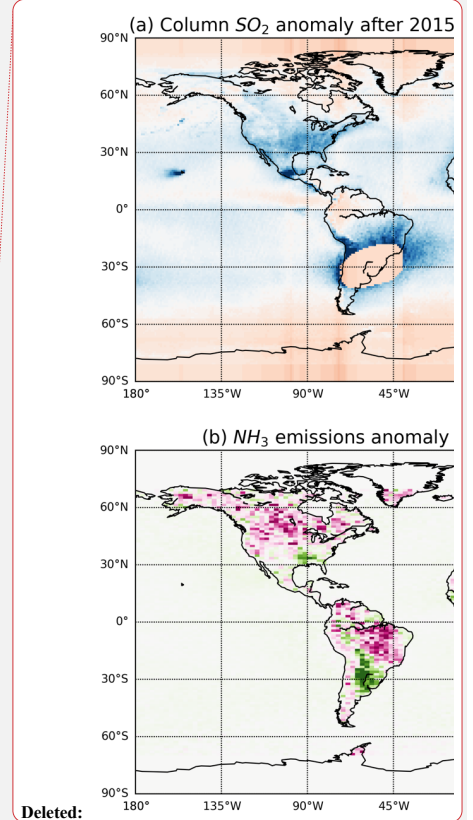
Deleted: nitrate



1355

1356 Figure 2. Annual average total column (a) sulfur dioxide and (b) nitrogen dioxide anomaly
 1357 after 2015 from OMI, and (c) annual average emission anomaly of ammonia calculated from
 1358 IASI in the present study (NE).

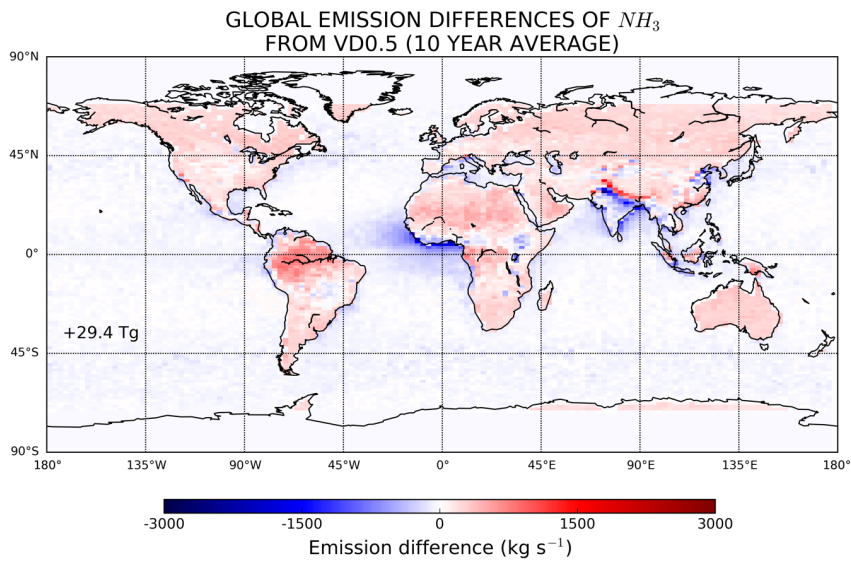
1359



Deleted: (a)

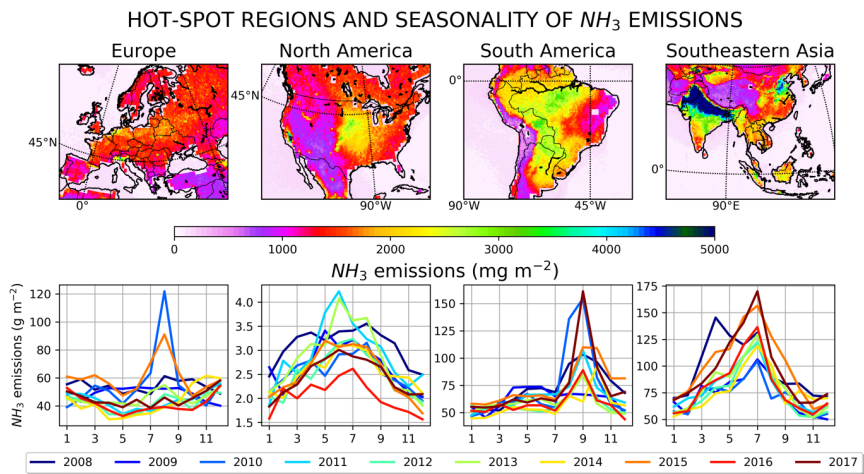
Deleted:

Deleted: b



1364
 1365 Figure 3. Global differences of ammonia emissions calculated in the present study (NE) from
 1366 those calculated using Van Damme et al. (2018) gridded concentrations applying a constant
 1367 lifetime of 0.5 days (VD0.5). The results are given as 10-year average (2008–2017) and the
 1368 number denotes the annual difference in the emissions.

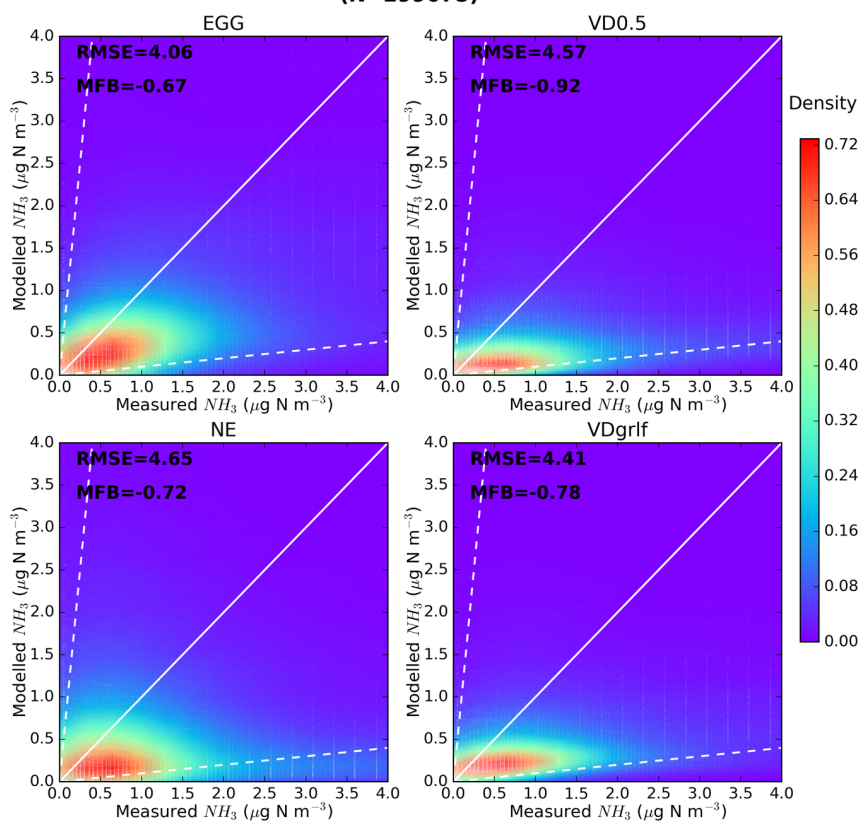
1369



1370
 1371 Figure 4. Total annual emissions of ammonia averaged over the 10-year period (2008–2017) in
 1372 Europe, North and South America and Southeastern Asia, which are regions characterized by
 1373 the largest contribution to global ammonia budget. In the bottom panels the monthly variation
 1374 of the emissions is shown for each year of the study period.

1375

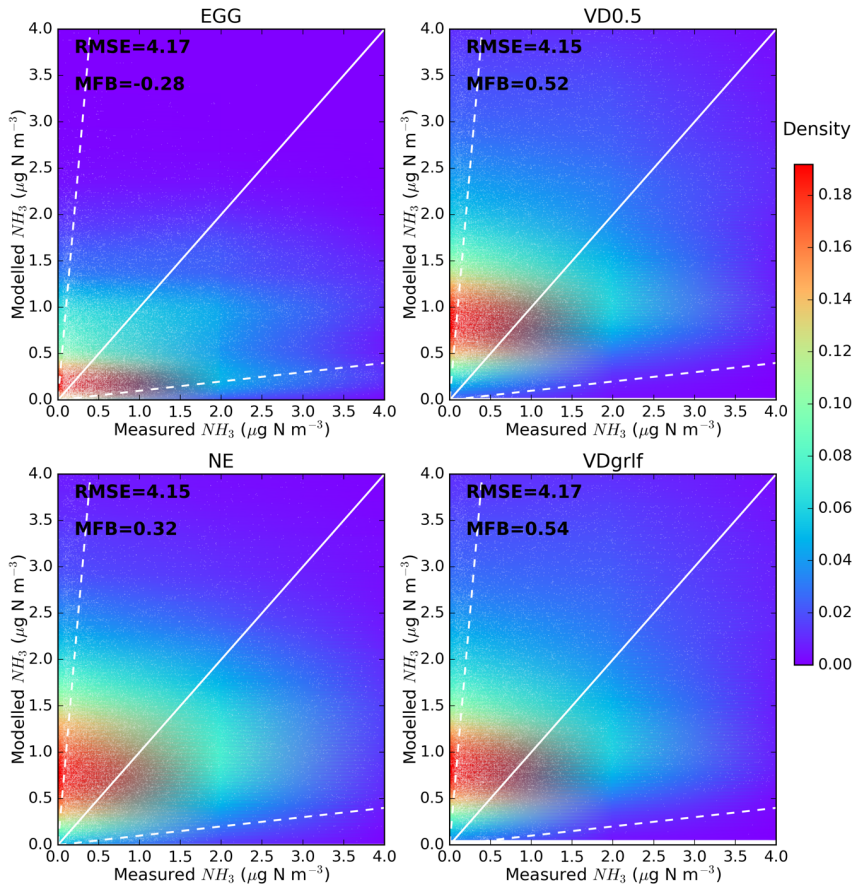
**COMPARISON WITH OBSERVATIONS FROM EMEP
(N=299075)**



1376
1377 Figure 5. Validation of modelled concentrations of ammonia for different emissions datasets
1378 (EGG, VD0.5, NE and VDgrif) against ground-based measurements from EMEP for the 10-
1379 year (2008–2017) study period. Scatterplots of modelled against measured concentrations for
1380 the aforementioned emission inventories were plotted with the Kernel density estimation, which
1381 is a way to estimate the probability density function (PDF) of a random variable in a non-
1382 parametric way.

1383

**COMPARISON WITH OBSERVATIONS FROM AMON
(N=27096)**

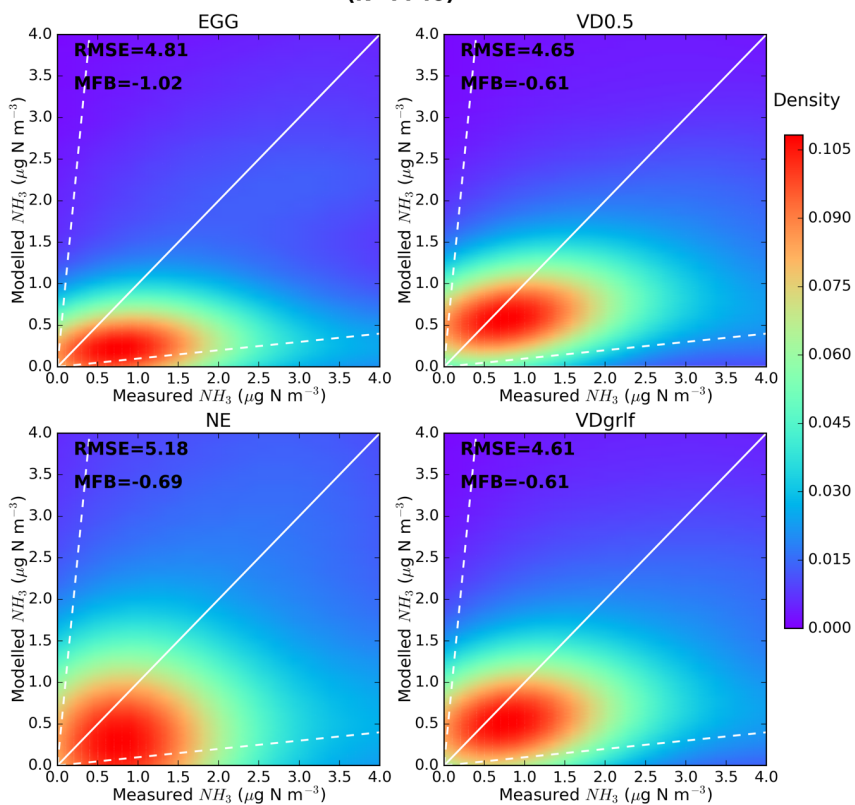


1384

1385 Figure 6. Validation of modelled concentrations of ammonia for different emissions datasets
 1386 (EGG, VD0.5, NE and VDgrlf) against ground-based measurements from AMON for the 10-
 1387 year (2008–2017) study period. Scatterplots of modelled against measured concentrations for
 1388 the aforementioned emission inventories were plotted with the Kernel density estimation, which
 1389 is a way to estimate the probability density function (PDF) of a random variable in a non-
 1390 parametric way.

1391

**COMPARISON WITH OBSERVATIONS FROM EANET
(N=7740)**

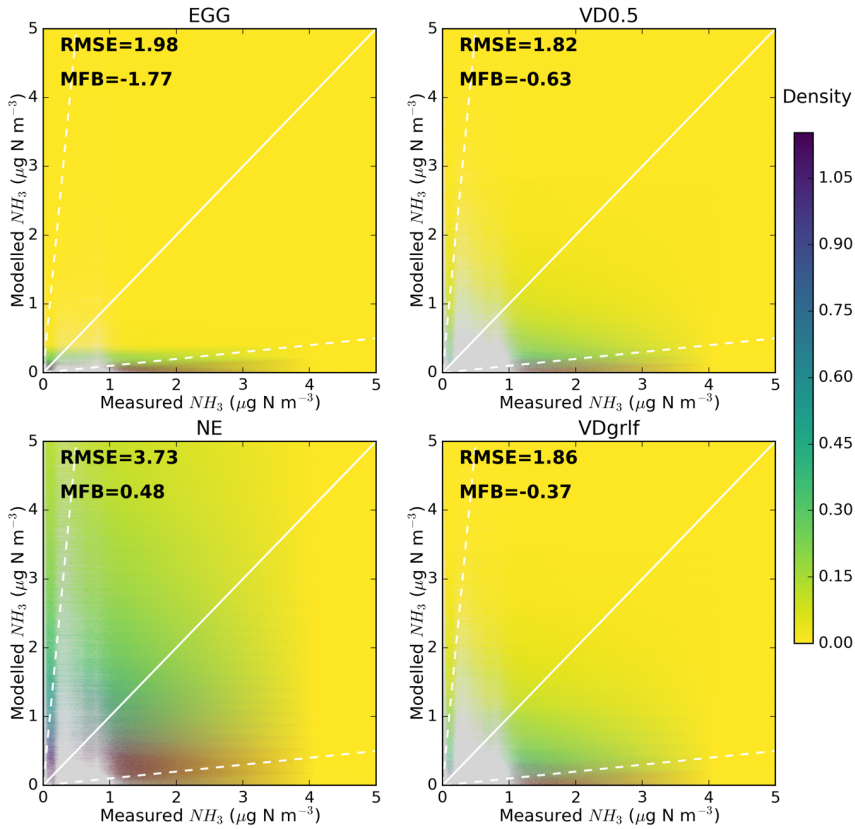


1392

1393 Figure 7. Validation of modelled concentrations of ammonia for different emissions datasets
 1394 (EGG, VD0.5, NE and VDgrlf) against ground-based measurements from EANET for the 10-
 1395 year (2008–2017) study period. Scatterplots of modelled against measured concentrations for
 1396 the aforementioned emission inventories were plotted with the Kernel density estimation, which
 1397 is a way to estimate the probability density function (PDF) of a random variable in a non-
 1398 parametric way.

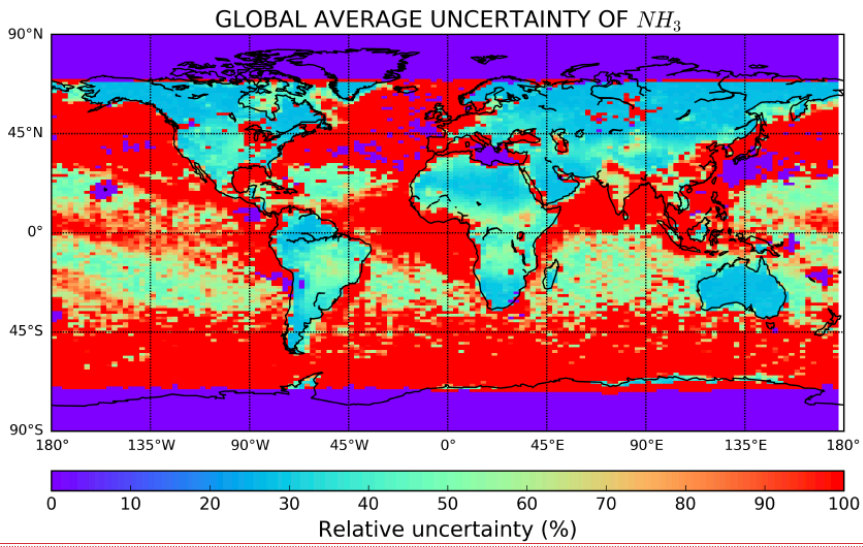
1399

**COMPARISON WITH OBSERVATIONS FROM CRIS
(N=4465037)**



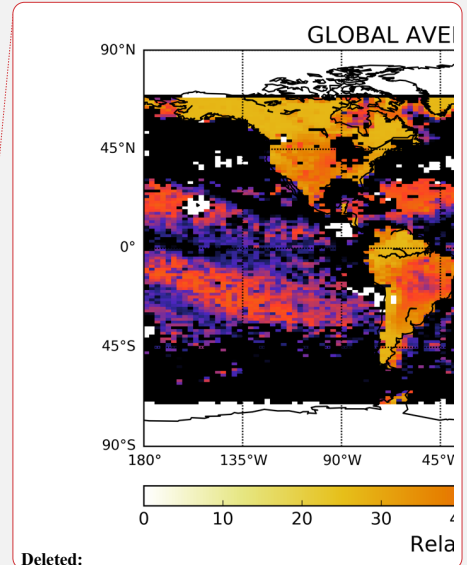
1400 Figure 8. Kernel density estimation (KDE) of the probability density function (PDF) of
 1401 modelled versus CrIS concentrations of ammonia in a non-parametric way. Modelled
 1402 concentrations are results of simulations using different emissions datasets (EGG, VD0.5, NE
 1403 and VDgrlf) for 2012–2017.
 1404

1405



1406
1407
1408
1409
1410

Figure 9. 10-year average relative uncertainty of modelled surface concentrations expressed as the standard deviation of surface concentrations from a model ensemble (Table 1) divided by the average.



Deleted:

Deleted: Table 1

1413 Table 1. Model ensemble simulations using different emissions for ammonia that were used in
 1414 the calculations of uncertainty. Uncertainties were calculated as the standard deviation of the
 1415 surface concentrations of ammonia from the 10 ensemble members for the 10-year period
 1416 (2008–2017).

	Parameter perturbed	10-year average emissions (Tg yr ⁻¹)
Ensemble 1	$d_k = 0$ in Eq. 2	121±50.6
Ensemble 2	$d_k = 10$ in Eq. 2	175±33.3
Ensemble 3	$d_k = 20$ in Eq. 2	189±28.7
Ensemble 4	$d_k = 60$ in Eq. 2	218±15.5
Ensemble 5	$d_k = 100$ in Eq. 2	208±51.8
Ensemble 6	$d_k = 500$ in Eq. 2	223±26.5
Ensemble 7	EGG	65±2.8
Ensemble 8	VD0.5	189
Ensemble 9	NE	213±18.1
Ensemble 10	VDgrlf	201±10.4

1417

1418

1419 **SUPPLEMENTARY FIGURE LEGENDS**

1420

1421 **Figure S 1.**

1422

1423 **Figure S 2.**

1424

1425 **Figure S 3.**

1426

1427 **Figure S 4.**

1428

1429 **Figure S 5.**

1430

1431 **Figure S 6.**

1432

1433 **Figure S 7.**

1434

1435 **Figure S 8.**

1436

1437 **Figure S 9.**

1438

1439 **Figure S 10.**

1440

1441 **Figure S 11.**